University of New Orleans

ScholarWorks@UNO

University of New Orleans Theses and Dissertations

Dissertations and Theses

Summer 8-2-2012

Electronic Transport in Thermoelectric Bismuth Telluride

Westly Nolting
wnolting@uno.edu

Follow this and additional works at: https://scholarworks.uno.edu/td

Part of the Condensed Matter Physics Commons

Recommended Citation

Nolting, Westly, "Electronic Transport in Thermoelectric Bismuth Telluride" (2012). *University of New Orleans Theses and Dissertations*. 1539.
https://scholarworks.uno.edu/td/1539

This Thesis-Restricted is protected by copyright and/or related rights. It has been brought to you by ScholarWorks@UNO with permission from the rights-holder(s). You are free to use this Thesis-Restricted in any way that is permitted by the copyright and related rights legislation that applies to your use. For other uses you need to obtain permission from the rights-holder(s) directly, unless additional rights are indicated by a Creative Commons license in the record and/or on the work itself.

This Thesis-Restricted has been accepted for inclusion in University of New Orleans Theses and Dissertations by an authorized administrator of ScholarWorks@UNO. For more information, please contact scholarworks@uno.edu.

Electronic Transport in Thermoelectric Bismuth Telluride

A Thesis

Submitted to the Graduate Faculty of the
University of New Orleans
in partial fulfillment of the
requirements for the degree of

Master of Science
in
Applied Physics

by

Westly Michael Nolting
B.S. University of New Orleans, 2010

August 2012

This UNO Master's Thesis was made possible with the help and support of many individuals. First and foremost I wish to offer my sincerest gratitude to my advisor, Dr. Kevin Stokes. He has been a monumental role model to me in the development of my ability to conduct research in the area of physics. He has supported me throughout my thesis with his guidance and knowledge all while still allowing me to develop my own methods in conducting research. Not only has he provided me support in my research but he has also been a great professor of physics with his classes helping me grasp the most fundamental topics in physics. Without his help this Master's thesis would not be possible. Thank you Dr. Kevin Stokes for all that you have done.

I would like to also thank my thesis committee members: Dr. Leszek Malkinski and Dr. Juliette Ioup. Dr. Leszek Malkinski has provided me with all my knowledge of solid state theory, which is a big part of this thesis. His classes have given me the confidence to even talk about condensed matter physics in this thesis, which is hard to come by when first starting research as a graduate student. Dr. Juliette Ioup has always been the most supportive and enthusiastic person in the Physics department. Any kind physics related problem that I needed help with she would always have such a cheerful and helpful outlook on ways to solve the problem. Dr. Juliette Ioup inspired me to always remember that I chose physics because it is a beautiful subject to learn and study.

I would like to thank Dr. Sumithra Santhanam and Dr. Rumana Yaqub for not only providing me the samples and materials needed to perform the experiments outlined in this thesis, but also for being wonderful co-workers. Despite all that they had on their list of things to do they would still help me if asked.

Advanced Materials Research Institute, AMRI, has provided me a job for these past years and truly without it my graduate career would have been a long and expensive endeavor. The Department of Physics has given me home for a long time now and the people within the department have brought me such joy in learning and working alongside them.

Finally I thank my family for giving me endless support and time in helping me pursue my goal of obtaining a master's degree. Without their shoulder to lean on and complain about life's problems and issues, my life would be immensely more difficult and less fulfilling.

Contents

Physical Constants **vii**

Symbols **viii**

Abstract **x**

1 Introduction **1**

1.1 Overview 1

1.2 The Hall Effect 2

1.3 Thermoelectrics 8

1.3.1 Properties of Thermoelectric Materials 8

1.3.2 Thermoelectric Applications 9

2 Background Theory **11**

2.1 Electronic Transport Theory 11

2.1.1 Electrical Conductivity 18

2.1.2 Weidemann-Franz Law 19

2.1.3 Seebeck Effect 20

2.2 Hall Effect 24

2.3 Scattering Parameter "r" 27

3 Experimental Setup **29**

3.1 Samples 29

3.2 Hall Effect 30

3.2.1 Geometry 30

3.2.2 Hall Equipment 34

3.2.3 Samples in Hall Effect Apparatus 36

3.2.4 Ohmic Contact Fabrication 37
3.2.5 Hall Data Analysis 38
3.3 ZEM Equipment 39

4 Results **41**
4.1 Structure of Bi_2Te_3/Bi Nanocomposite 41
4.2 Electronic Transport Measurements 41
4.3 Electron Filtering Results 46

5 Conclusions **48**
5.1 Conclusion 48

A Fermi Integral values **50**

B Bi2Te3 solid state constant values **52**

C Seebeck Coefficient and Carrier Concentration Values **54**

D Lakeshore 370/3708 Voltage Ranges **58**

E Lakeshore 455 RMS operation range **61**

F Field vs. Gap for GMW Electromagnet **62**

G CRM Stainless Steel **63**

Bibliography **64**

Vita **66**

List of Figures

1.1 Lorentz Force . . . 3
1.2 Hall effect wire diagram . . . 4
1.3 Basic Thermoelectric Device . . . 10

3.1 Hall bar geometry . . . 30
3.2 Hall bar with 5 contacts . . . 32
3.3 Van der Pauw diagram . . . 33
3.4 Hall Apparatus . . . 34
3.5 Hall Effect Diagram . . . 35
3.6 Sample Stage . . . 37
3.7 Hall Data Anaylsis . . . 38
3.8 ZEM3 Sample Stage . . . 40

4.1 Carrier and Mobility Plot . . . 43
4.2 Conductivity Plot . . . 44
4.3 Seebeck Coefficient Plot . . . 45
4.4 Piseranko Plot . . . 46

F.1 GMW Field Gap . . . 62

List of Tables

4.1 Table of Measured and Calculated Values 42

A.1 Fermi-Integral Values 51

B.1 General properties of Bi_2Te_3 52
B.2 Electrical, optical, and thermal properties of Bi_2Te_3 53

C.1 Seebeck coefficient and carrier concentration values for pisarenko plot. 55
C.2 Seebeck coefficient and carrier concentration values for pisarenko plot. 56
C.3 Seebeck coefficient and carrier concentration values for pisarenko plot. 57

D.1 Lakeshore 370/3708 Voltage Range 58
D.2 Lakeshore 370/3708 Voltage Range cont. 59
D.3 Lakeshore 370/3708 Voltage Range cont. 60

E.1 The Lakeshore 455 DPS Gaussmeter operation ranges from the Lakeshore 455 manual for the High Sensitivity Probe (HSE). 61

G.1 Table of thermal conductivity and electrical resistivity 63

Physical Constants

Speed of Light	c	=	$2.997\ 924\ 58 \times 10^{8}$ $\mathrm{ms}^{-\mathrm{S}}$ (exact)
Boltzmann constant	k_B	=	$1.3807 \times 10^{-23} m^2 \cdot kg \cdot s^{-2} \cdot K^{-1}$
Planck's constant	$\hbar$	=	$1.0546 \times 10^{-34} J \cdot s$
Scattering parameter	r	=	$-\frac{1}{2}, 0, \frac{1}{2}, 1, \frac{3}{2}$
Lorentz' number	L	=	$2.45 \times 10^{-8} W \cdot \Omega \cdot K^{-2}$

Symbols

A	Area	m^2
$\vec{B}$	Magnetic field	T
c	speed of light	$m \cdot s^{-1}$
C_e	specific heat	$J \cdot K^{-1} \cdot kg^{-1}$
$D(E)$	density of states	$J^{-1} \cdot m^{-3}$
E	energy	J
$\vec{\mathcal{E}}$	Electric field	$kg \cdot m \cdot s^{-3} \cdot A^{-1}$
E_x	Electric field in the x-direction	$kg \cdot m \cdot s^{-3} \cdot A^{-1}$
E_y	Electric field in the y-direction	$kg \cdot m \cdot s^{-3} \cdot A^{-1}$
E_z	Electric field in the z-direction	$kg \cdot m \cdot s^{-3} \cdot A^{-1}$
f	distribution function	unit less
f_0	Fermi-Dirac distribution function	unit less
$\vec{F}$	Force	$kg \cdot ms^{-2}$
$\vec{F_E}$	Force of the electric field	$kg \cdot ms^{-2}$
$\vec{F_B}$	Force of the magnetic field	$kg \cdot ms^{-2}$
I	current	A
J	current density	$A \cdot m^{-2}$
J_x	charge flux in the x-direction	$A \cdot m^{-2}$
J_{Ex}	energy flux in the x-direction	
k_e	thermal conductivity	$W \cdot m^{-1} \cdot K^{-1}$
n	carrier concentration	m^{-3}
$\vec{p}$	momentum	$kg \cdot m \cdot s^{-1}$
q	charge	C

r	position	m
r	scattering parameter	unit less
R_H	Hall coefficient	$m^3 \cdot C^{-1}$
S	Seebeck coefficient	$V \cdot K^{-1}$
t	thickness	m
T	temperature	K
$\vec{v}$	velocity	$m \cdot s^{-1}$
V	Voltage	V
V_H	Hall Voltage	V
v_d	drift velocity	$m \cdot s^{-1}$
w	width	m
ζ	reduced energy	unit less
η	location of Fermi energy level with respect to the conduction band	unit less
μ	chemical potential	J
μ_e	electron mobility	$m^2 \cdot V^{-1} \cdot s^{-1}$
μ_H	Hall mobility	$m^2 \cdot V^{-1} \cdot s^{-1}$
ρ	resistivity	$\Omega \cdot m$
σ	conductivity	$S \cdot m^{-1}$
Ω	Volume	m^3
τ	relaxation time	s
Φ	electrochemical potential	J
ϕ_e	electric potential	J

Abstract

An experimental investigation of the electronic transport properties of bismuth telluride nanocomposite materials is presented. The primary transport measurements are electrical conductivity, Seebeck coefficient and Hall effect. An experimental apparatus for measuring Hall effect and electrical conductivity was designed, constructed and tested. Seebeck coefficient measurements were performed on a commercial instrument. The Hall effect and Seebeck coefficient measurements are two of the most important tools for characterizing thermoelectric materials and are widely used in the semiconductor industry for determining carrier types, carrier concentration and mobility. Further, these transport parameters are used to determine the thermal to electrical conversion efficiency of a thermoelectric material. The Boltzmann transport equation was used to analyze the Seebeck coefficient, carrier mobility and electrical conductivity as a function of carrier concentration for eleven samples. The relationship between the electronic transport and material/composite composition is discussed.

Bismuth, bismuth telluride, Boltzmann equation, carrier concentration, conductivity, electronic transport, figure of merit, mobility, Seebeck coefficient, semiconductor.

Chapter 1

INTRODUCTION

1.1 Overview

Thermoelectric materials are materials that can convert heat to electrical energy or, the converse of this effect, use electrical current to move heat. The materials are used in variety of power generation and solid state cooling devices. [1] A measure of a material's ability convert heat to electrical energy (or vice versa) is the "figure of merit" Z given by

$$Z = \frac{S^2\sigma}{\kappa}, \tag{1.1.1}$$

where S is the Seebeck coefficient, σ is the electrical conductivity and κ is the total thermal conductivity (sum of the electronic and lattice thermal conductivities). The figure of merit is related to the efficiency for power generation and the coefficient of performance for refrigeration. High efficiency or high coefficient of performance require high Z. Multiplying Z times the absolute temperature T gives a dimensionless figure of merit ZT; ZT>1 is required for most practical applications. Not surprisingly, in the thermoelectric field of physics, characterization of materials requires accurate measurements of the Seebeck coefficient, electrical conductivity, and thermal conductivity.

Clearly, a good thermoelectric material requires both a high Seebeck coefficient and a high electrical conductivity. Both the Seebeck coefficient and the electrical conductivity are sensitive functions of the carrier concentration n. In semiconductor materials the electrical conductivity increases with increasing carrier concentration. Unfortunately, the Seebeck coefficient decreases with increasing carrier concentration. Much thermoelectric research is aimed at optimizing the value of by adjusting the carrier concentration. The carrier concentration is determined from a fourth measurement, the Hall effect. This thesis experimentally investigates the electronic transport in bismuth telluride, Bi_2Te_3, and nanocomposites formed from Bi_2Te_3. The primary topics of the thesis are the design, construction and testing of a Hall effect measurement system, Hall effect measurements and the analysis of the relationship between S, σ and n for a series of Bi_2Te_3 nanocomposites

1.2 The Hall Effect

Eighteen years before anyone understood what an electron was or that they existed, back when current was thought to be an incompressible fluid, Edwin Hall, while working on his dissertation, discovered that when applying a current along thin gold leaf attached to a glass slide, there was no voltage read perpendicular to the current, but when the gold leaf slide was placed between the poles of a magnet, a transverse voltage appeared. [2]

He believed that this phenomenon to be a new electromotive force that appeared at right angles to the primary electromotive force. This new force was labelled by him as the transverse electromotive force, and he found that it was proportional to the product of current per area and magnetic field.It was more famously known later as the Lorentz Force.

Consider a stream of electrons confined to the dimensions of a solid with velocity, $\vec{v}$, in the x-direction as shown in Fig. 1.1. An applied magnetic field in the z-direction will deflect the flow of electrons into the y-direction causing an unbalanced charge distribution within the solid, creating an electric field $\mathcal{E}_y$. Eventually as the charges build up on the side of the solid that is being deflected towards, the forces from the magnetic and electric fields balance

and the charges are no longer deflected and a steady-state exists.[3] This is the Hall effect. Measurement of this transverse potential difference along with the electrical conductivity provides a way to measure the carrier concentration and carrier type in a semi-conductor or conductor.

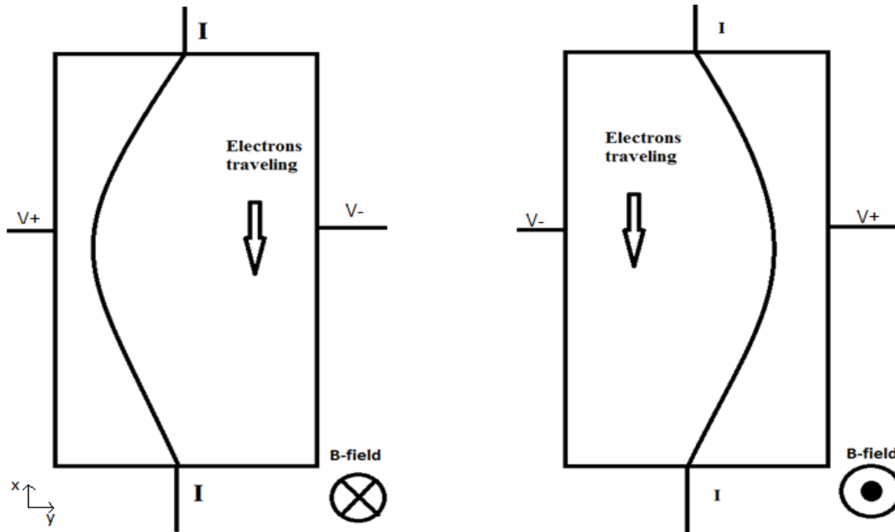

FIGURE 1.1: The Lorentz force demonstrated in a Hall bar geometry.

The underlying principle of the Hall effect is a potential difference that is created when a current carrying material is placed with the current perpendicular to a magnetic field. This causes a deflection in the current and in turn causes an electric potential to appear. This difference in potential and deflection of electrons are caused by the Lorentz Force given by

$$\vec{F} = q(\vec{\mathcal{E}} + \vec{v} \times \vec{B}). \tag{1.2.1}$$

Consider a current passing through a material in the x-direction, as shown in Fig. 1.2. An applied magnetic field oriented in the z-direction causes an electric field to build up in the y-direction due to the deflection of charge carriers. This build up of electric field is called the Hall voltage and is equal to the electric field times the width w of the strip.

$$V_H = \mathcal{E}_y w \tag{1.2.2}$$

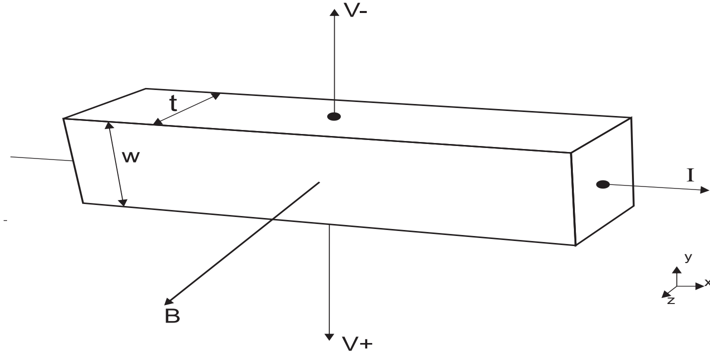

FIGURE 1.2: The basic wire setup for the Hall bar geometry

When there is no magnetic field the Hall voltage measured across the sample from V+ to V- is nearly zero. If all wires and contacts are placed perfectly the voltage measured could be zero, but in practice it is just very close to zero.

As before, $\vec{\mathcal{E}}$ is the electric field, v is the velocity of the electrons, q is the charge of an electron, and $\vec{B}$ is the applied magnetic field. The right-hand rule can be used to find the direction of the magnetic force that is acting on the electron. To get the basic equations of the Hall effect from the Lorentz force, the electric and magnetic field components of the force must be equal. The force due to the magnetic field $\vec{B}$ is

$$\vec{F}_B = q(\vec{v} \times \vec{B}). \tag{1.2.3}$$

When measuring the Hall effect, the velocity of the electrons and the magnetic field are perpendicular resulting in $\vec{v} \times \vec{B} = vB$

$$F_B = qv_dB, \tag{1.2.4}$$

where v_d is the electron drift velocity within a solid due to the electrical current flowing through the solid. The force due to the electric field $\mathcal{E}$ is

$$F_E = q\mathcal{E}. \tag{1.2.5}$$

Now we can equate the two and extract an expression of the electric field in terms of the applied magnetic field:

$$\begin{aligned} F_E &= F_B \\ q\mathcal{E} &= qv_dB \\ \mathcal{E} &= v_dB \end{aligned} \tag{1.2.6}$$

This field equation is similar to the relationship between the electric field and magnetic field for electromagnetic radiation, $\mathcal{E} = cB$, with c being the speed of light. Next the drift velocity is defined as the ratio of current density to carrier concentration and electric charge:

$$\begin{aligned} v_d &= \frac{J}{ne} \\ J &= \frac{I}{A} \\ v_d &= \frac{I}{neA} \end{aligned} \tag{1.2.7}$$

with A being the cross-sectional area of the sample. Equations 1.2.6 and 1.2.7 can be combined to produce the Hall voltage:

$$V_H = \frac{IBw}{neA} = \frac{IB}{ent} \tag{1.2.8}$$

with t being the thickness of the sample from Fig. 1.2. When measuring the carrier concentration it is good to keep in mind that there are two types of charge carriers: holes and electrons, or p-type and n-type, respectively. These carrier types can be determined by the sign of the Hall coefficient R_H defined as

$$R_H = \frac{V_H t}{I_x B_z}. \quad (1.2.9)$$

The sign of R_H indicates whether the material is p-type (+ sign) or n-type (- sign). In n-type materials the carriers are electrons donated by impurity atoms that are capable of giving up extra electrons to the primary material. This act of doping raises the carrier concentration. For example, in silicon, phosphorous acts as a donor creating n-type silicon. Silicon, a group 14 element, has four valance electrons, and phosphorous, a group 15 element, has five valance electrons. The four electrons from each silicon atom are able to form covalent bonds while the last fifth electron from phosphorous is unpaired and forms a weak bond, allowing it to move freely, giving extra negative charge carriers.

When describing p-type materials, it is correct to assume an opposite response to that of n-type materials. P-type semiconductors can be considered as acceptor material. This means that when a dopant is present in the primary material there is a *lack* of bond with the host material, or a missing bond. Silicon and aluminium are good examples of this. When aluminum is used as a dopant, the four electrons from silicon are only able to form three covalent bonds with the three electrons from the aluminum, thus creating a hole. This hole is able to attract electrons from the closest neighboring atoms. One electron from a neighbor moves into the hole, which now on the neighboring atom. The process is repeated. This can create the illusion of the hole traveling around the material carrying current and therefore acting as a charge carrier. [4]

Narrow-gap semiconductors like bismuth telluride are often doped by forming off-stoichiometric compounds, like $Bi_{2-x}Te_{3+x}$. In this case, excess Te (a group 16 element) has six valance electrons paired with bismuth (a group 15 element with five valance electrons), resulting in a p-type material. Similarly, excess bismuth will result in an n-type material. The number of charge carriers is

$$n = \frac{1}{R_H q}. \quad (1.2.10)$$

Along with knowing the type of carrier, the Hall coefficient and the resistivity can produce a value for the mobility of the carriers. The fundamental equation for electrical conductivity can be written

$$\sigma = qn\mu_e, \tag{1.2.11}$$

where μ_e is the carrier mobility. Mobility is the ability of an electron to move through a semiconductor or metal when in the presence of an electric field. The intrinsic or conductivity mobility appears in the equation above. We can use the Hall effect to measure a related quantity, the Hall mobility μ_H. Combining Eq.1.2.11 with Eq. 1.2.10 yields

$$\sigma = q\left(\frac{1}{R_H q}\right)\mu_H = \frac{\mu_H}{R_H} \tag{1.2.12}$$

or

$$\mu_H = \sigma R_H. \tag{1.2.13}$$

The importance of mobility stems from its use in building electronic devices. When the carrier mobility of a semiconductor is high, the material is able to carry a higher current allowing the device material to have a greater time response. When the material is in the presence of a small or low electric field the velocities of the electrons are proportional to the mobility, meaning when the mobility is higher a low electric field electron velocity is able to produce a higher time response. This higher response time means that semiconductors with high mobility may be used in high frequency applications.

These properties of the Hall effect are important for the characterization of semiconductors. Semiconductors have become more important as more and more applications are found. Semiconductors can be excellent thermoelectric materials when they are heavily doped to have carrier concentrations resembling those of metals.[5] Some of the best thermoelectric semiconductors are those from the group 15 elements (bismuth and antimony) combined with group 16 elements (tellurium and sellenium). [6]

1.3 Thermoelectrics

In 1821 the Seebeck effect was discovered by T.J. Seebeck when he noticed that a compass needle was deflected when a metal was heated with a heat gradient. He called the effect thermomagnetism. Oersted later redefined it when he observed that an electric current is able to produce a magnetic field and gave it the correct name of thermoelectricity. [7]

Thermoelectric devices can convert electrical energy into a temperature gradient. The application of this cooling or heating effect remained minimal until the development of semiconductor materials. With the advent of semiconductor materials came the capability for a wide variety of practical thermoelectric refrigeration methods. [8]

1.3.1 Properties of Thermoelectric Materials

If a temperature gradient is established across a semiconductor material, a voltage is created by the change in temperature. This voltage is the Seebeck voltage. When this voltage is compared to the temperature gradient, the Seebeck coefficient S can be determined:

$$S = \frac{\Delta V}{\Delta T}. \tag{1.3.1}$$

With V being the voltage from the temperature gradient and T the temperature. This is the basis of thermoelectric power generation.

Related to the Seebeck effect is the Peltier effect. This effect was named after Jean-Charles Peltier and was discovered in 1834. Peltier discovered that if a current flows through specific materials a temperature gradient is created at two junctions of the material. This means that if a current passes through two thermoelectric materials, one side of the material will heat up while the other side cools down. This is the ground work for developing thermoelectric cooling devices.

1.3.2 Thermoelectric Applications

When talking about thermoelectric applications, it is important to mention that most applications involve a thermoelectric module. This module could be a small or large device that has thermoelectric elements and contains two different types of thermoelectric materials. One material is an n-type material and the other is a p-type, often called a "unicouple."

One unicouple is shown in Fig. 1.3. A module consists of alternating n- and p-type thermoelectric elements. The combination of both carrier type semiconductors means that the heat is carried in one direction only due to each material having a different free electron density at the same local temperature. These modules usually a have symmetrical number of each carrier type. The change in temperature between n- and p-type occurs when the current moves to a different carrier type. Current transferring to the n-type material causes the material to be heated since the n-type material has excess electrons. When the current transfers to the p-type material, the semiconductor that is lacking free electrons, is cooled. These materials changing temperature causes the cold side of the module to become colder and the hot side to become hotter.[1]

In Figure 1.3 only a small part of a thermoelectric module is shown. This basic setup is replicated several times to make the full module.

These modules are used in many cooling applications. Probably one of the biggest applications is for cooling electronic devices. Since the current is already present to power the device, it is relatively easy to incorporate a module to cool the heat-producing electronics. Cooling the device can help eliminate thermal noise in the circuitry and improve the accuracy of the electronic instruments.

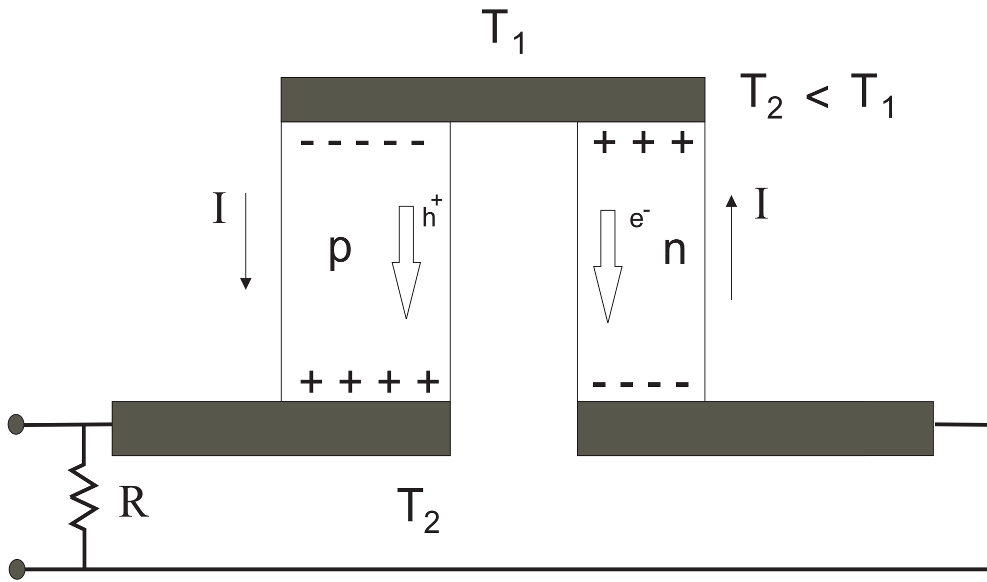

Figure 1.3: Basic configuration of a thermoelectric generator. The black connecting bars are solder which electrically connect the two carrier types, this allows flow of the current throughout the module which is created by the heat being supplied at the top. [5]

The number of thermoelectric modules used as refrigerators and air conditioners has increased over the past few years. Refrigerators and air conditioners have been converting from the chlorofluorocarbon (CFC) type of air cooling to thermoelectric cooling. One of the main reasons is that the CFC's released into the atmosphere has been linked to damaging effects for the upper atmosphere.

Chapter 2

BACKGROUND THEORY

In this chapter, the theory behind electronic transport will be explained, as well as the supporting topics associated with it: Hall effect, Seebeck effect, conductivity, and the Weidermann-France Law. All the transport equations described can be derived from the Boltzmann transport equation.

2.1 Electronic Transport Theory

The derivation presented here follows Arabshahi and Sarlak. [9] The Boltzmann transport equation is analogous to Schroedinger's equation but describes the variation of the electronic distribution function f over time. f is also called the probability of occupation of states. The Boltzmann transport equation is a robust and widely applicable equation used to derive all of the transport parameters.[10]

The Boltzmann transport equation is [10]

$$\frac{df}{dt} = \left.\frac{\partial f}{\partial t}\right|_{coll}, \tag{2.1.1}$$

which states that the change in distribution function with respect to time equals the change in distribution function due to collisions. The equation can be expanded as

$$\frac{\partial f}{\partial t} + \frac{\partial f}{\partial \vec{p}}\frac{d\vec{p}}{dt} + \frac{\partial f}{\partial \vec{r}}\frac{d\vec{r}}{dt} = \left.\frac{\partial f}{\partial t}\right|_{coll}. \tag{2.1.2}$$

The expansion is in terms of momentum and position because the end result of a transport equation is to know the velocity of the carriers as a function of position. Note that $d\vec{p}/dt$ is the electric force and $d\vec{r}/dt$ is the velocity $\vec{v}$ of electrons. Although this is a complete equation, when considering scattering and a relaxation time approximation must be used. That is, we assume the time derivative of the distribution function is proportional to the deviation of the distribution function from the equilibrium distribution function f_0

$$\left.\frac{\partial f}{\partial t}\right|_{coll} = -\frac{f - f_0}{\tau}. \tag{2.1.3}$$

This is the relaxation time approximation where τ is the relaxation time. Equation 2.1.2 becomes

$$\frac{\partial f}{\partial t} + \vec{v} \cdot \nabla f + q\vec{\mathcal{E}} \cdot \frac{\partial f}{\partial \vec{p}} = \frac{f_0 - f}{\tau} \tag{2.1.4}$$

In the above equation, $\frac{\partial f}{\partial t} = 0$ because the change in time of the distribution function is much smaller than the change in space of the distribution function, or $\frac{\partial f}{\partial t} << \frac{\partial f}{\partial r}$. Furthermore, in the Fermi-dirac distribution, f_0, the electric field variation is small and the temperature gradient within the solid is negligible so the change in the equilibrium is small, making $f = f_0$. Also the change in distribution with respect to time can be re-written as

$$\frac{\partial f_0}{\partial \vec{p}} = \frac{\partial f_0}{\partial E}\frac{dE}{d\vec{p}} = \vec{v}\frac{\partial f_0}{\partial E}. \tag{2.1.5}$$

Since $\vec{p} = m\vec{v}$ and $E = p^2/2m$, the derivative of energy with respect to momentum is the velocity.

The Boltzmann equation with the time relaxation approximation is

$$\vec{v} \cdot [\nabla f_0 + q\vec{\mathcal{E}}\frac{\partial f_0}{\partial E}] = \frac{f_0 - f}{\tau}, \tag{2.1.6}$$

where f_0 is the Fermi-Dirac distribution

$$f_0(\vec{k}) = \frac{1}{e^{\frac{E(\vec{k})-\mu}{k_B T}} + 1}. \tag{2.1.7}$$

Now equation 2.1.6 can be simplified. Starting with the derivative of the Fermi-Dirac distribution, and using the chain rule the term becomes

$$\frac{\partial f_0}{\partial E} = \frac{df_0}{d\eta}\frac{\partial \eta}{\partial E} = \frac{df_0}{d\eta}\frac{1}{k_B T}; \frac{df_0}{d\eta} = k_B T \frac{\partial f_0}{\partial E}, \tag{2.1.8}$$

where η is the location of the Fermi energy level with respect to the conduction band. The change in distribution in space is

$$\nabla f_0 = \frac{df_0}{d\eta}\nabla\eta = k_B T \frac{\partial f_0}{\partial E}. \tag{2.1.9}$$

Then

$$\nabla\eta = \frac{1}{k_B T}(\nabla E(\vec{k}) - \nabla\mu) - \frac{E-\mu}{k_B T^2}\nabla T = -\frac{1}{k_B T}\nabla\mu - \frac{E-\mu}{k_B T^2}\nabla T \tag{2.1.10}$$

and

$$\nabla f_0 = -\frac{\partial f_0}{\partial E}(\nabla\mu + \frac{E-\mu}{T}\nabla T). \tag{2.1.11}$$

Equation 2.1.6 is now expanded to

$$\vec{v} \cdot [-\nabla\mu - \frac{E-\mu}{T}\nabla T + q\vec{E}]\frac{\partial f_0}{\partial E} = \frac{f_0 - f}{\tau}. \tag{2.1.12}$$

The electric field can also be written as

$$\vec{\mathcal{E}} = -\nabla\phi_e \tag{2.1.13}$$

Where ϕ_e is the electric potential. Then equation 2.1.12 becomes

$$\vec{v} \cdot [-\nabla\mu - \frac{E-\mu}{T}\nabla T - q\nabla\phi_e]\frac{\partial f_0}{\partial E} = \frac{f_0 - f}{\tau}. \tag{2.1.14}$$

Now that the electric field is in terms of a potential, the electrochemical potential can be defined to be just the sum of the chemical potential μ and the electrostatic potential ϕ_e: $\Phi = \mu + q\phi_e$.

Equation 2.1.14 is solved for the first order distribution:

$$f = f_0 - \tau\vec{v} \cdot [-\nabla\Phi - \frac{E-\mu}{T}\nabla T]\frac{\partial f_0}{\partial E}. \tag{2.1.15}$$

The gradients in equation 2.1.15 are applied in the x-direction

$$\begin{aligned} f =& f_0 - \tau v\cos\theta[-\frac{d\mu}{dX} - \frac{E-\mu}{T}\frac{dT}{dX} + qE_x]\frac{\partial f_0}{\partial E} \\ =& f_0 - \tau v\cos\theta[-\frac{d\Phi}{dX} - \frac{E-\mu}{T}\frac{dT}{dX}]\frac{\partial f_0}{\partial E}. \end{aligned} \tag{2.1.16}$$

The charge flux and energy flux are now calculated. These two values will help in deriving the Seebeck coefficient and the conductivity. When calculating these flux values, a distribution of electrons f is considered within a small range of energies for the electrons. These small distribution of electrons and energies are associated with the density of states, thus the number of electrons is $fD(E)dE$. Since the electrons that are being considered are inside a solid, they will have an equal probability to move in any direction. This direction can be defined as a solid angle, $d\Omega$, from a point of origin. The probability that an electron will move within the solid angle of a sphere is $d\Omega/4\pi$. The movement of electrons in the solid causes a flux of charges equal to $qv\cos\theta$ and an energy flux of $Ev\cos\theta$. The charge flux and energy flux are

$$J_x = \int_{\phi=0}^{2\pi} \frac{d\phi}{4\pi} \int_{\theta=0}^{\pi} \sin\theta\cos\theta d\theta \int_{E=0}^{\infty} (fD(E))(qv)dE \tag{2.1.17}$$

and

$$J_{Ex} = \int_{\phi=0}^{2\pi} \frac{d\phi}{4\pi} \int_{\theta=0}^{\pi} \sin\theta\cos\theta d\theta \int_{E=0}^{\infty} (fD(E))(Ev)dE. \tag{2.1.18}$$

Substituting the charge flux into equation 2.1.16 will result in

$$\begin{aligned} J_x = & \int_{\phi=0}^{2\pi} \frac{d\phi}{4\pi} \int_{\theta=0}^{\pi} \sin\theta\cos\theta d\theta \int_{E=0}^{\infty} f_0 D(E)(qv)dE \\ & + \int_{\phi=0}^{2\pi} \frac{d\phi}{4\pi} \int_{\theta=0}^{\pi} \sin\theta\cos^2\theta d\theta \int_{E=0}^{\infty} D(E)(\tau q v^2[\frac{d\mu}{dX} + \frac{E-\mu}{T}\frac{dT}{dX} - qE_x]\frac{\partial f_0}{\partial E})dE \end{aligned} \tag{2.1.19}$$

$$\begin{aligned} J_{Ex} = & \int_{\phi=0}^{2\pi} \frac{d\phi}{4\pi} \int_{\theta=0}^{\pi} \sin\theta\cos\theta d\theta \int_{E=0}^{\infty} f_0 D(E)(Ev)dE \\ & + \int_{\phi=0}^{2\pi} \frac{d\phi}{4\pi} \int_{\theta=0}^{\pi} \sin\theta\cos^2\theta d\theta \int_{E=0}^{\infty} D(E)(\tau E v^2[\frac{d\mu}{dX} + \frac{E-\mu}{T}\frac{dT}{dX} - qE_x]\frac{\partial f_0}{\partial E})dE \end{aligned} \tag{2.1.20}$$

The first term in equations 2.1.19 and 2.1.20 both equal zero when integrated, so that

$$J_x = \frac{1}{3}\int_{E=0}^{\infty} D(E)(\tau q v^2[\frac{d\mu}{dX} + \frac{E-\mu}{T}\frac{dT}{dX} - qE_x]\frac{\partial f_0}{\partial E})dE \tag{2.1.21}$$

and

$$J_{Ex} = \frac{1}{3}\int_{E=0}^{\infty} D(E)(\tau E v^2[\frac{d\mu}{dX} + \frac{E-\mu}{T}\frac{dT}{dX} - qE_x]\frac{\partial f_0}{\partial E})dE. \tag{2.1.22}$$

v can be removed by using the kinetic energy

$$E = \frac{1}{2}mv^2 \tag{2.1.23}$$

resulting in

$$J_x = \frac{2q}{3m} \int\limits_{E=0}^{\infty} D(E)(\tau E[\frac{d\mu}{dX} + \frac{E-\mu}{T}\frac{dT}{dX} - qE_x]\frac{\partial f_0}{\partial E})dE \tag{2.1.24}$$

and

$$J_{Ex} = \frac{2}{3m} \int\limits_{E=0}^{\infty} D(E)(\tau E^2[\frac{d\mu}{dX} + \frac{E-\mu}{T}\frac{dT}{dX} - qE_x]\frac{\partial f_0}{\partial E})dE. \tag{2.1.25}$$

Separating terms for the electrochemical potential, equation 2.1.25 can be written as two integrals:

$$\begin{aligned}
J_{Ex} =& \frac{2}{3m} \int\limits_{E=0}^{\infty} D(E)(\tau E^2[\frac{d\mu}{dX} + \frac{E-\mu}{T}\frac{dT}{dX} - qE_x]\frac{\partial f_0}{\partial E})dE \\
=& \frac{2}{3m} \int\limits_{E=0}^{\infty} D(E)(\tau E(E-\mu)[\frac{d\mu}{dX} + \frac{E-\mu}{T}\frac{dT}{dX} - qE_x]\frac{\partial f_0}{\partial E})dE \\
&+ \mu\frac{2}{3m} \int\limits_{E=0}^{\infty} D(E)(\tau E[\frac{d\mu}{dX} + \frac{E-\mu}{T}\frac{dT}{dX} - qE_x]\frac{\partial f_0}{\partial E})dE \\
=& \frac{2}{3m} \int\limits_{E=0}^{\infty} D(E)(\tau E(E-\mu)[\frac{d\mu}{dX} + \frac{E-\mu}{T}\frac{dT}{dX} - qE_x]\frac{\partial f_0}{\partial E})dE + \frac{\mu J_z}{q} \\
=& \frac{2}{3m} \int\limits_{E=0}^{\infty} D(E)(\tau E(E-\mu)[\frac{d\Phi}{dX} + \frac{E-\mu}{T}\frac{dT}{dX}]\frac{\partial f_0}{\partial E})dE + \frac{\mu J_z}{q}
\end{aligned} \tag{2.1.26}$$

When the temperature is at zero kelvin (T=0K) the energy flux will be reduced to

$$J_{Ex} = \frac{\mu J_x}{q} \tag{2.1.27}$$

The thermal energy is the difference in energy flux at T = 0K and when T $\neq$ 0K:

$$
\begin{aligned}
J_{q_x} &= J_{Ex}(T) - J_{Ex}(T=0) \\
&= \frac{2}{3m} \int_{E=0}^{\infty} \frac{\partial f_0}{\partial E} D(E) E (E - E_F) \tau \left(\frac{d\Phi}{dX} + \frac{E-\mu}{T}\frac{dT}{dX}\right).
\end{aligned}
\tag{2.1.28}
$$

Combining terms under the same integral simplifies equation 2.1.24 to

$$
J_x = L_{11}\left(-\frac{1}{q}\frac{d\Phi}{dX}\right) + L_{12}\left(-\frac{dT}{dX}\right) \tag{2.1.29}
$$

and

$$
J_{q_x} = L_{21}\left(-\frac{1}{q}\frac{d\Phi}{dX}\right) + L_{22}\left(-\frac{dT}{dX}\right), \tag{2.1.30}
$$

where

$$
L_{11} = -\frac{2q^2}{3m} \int_{E=0}^{\infty} \frac{\partial f_0}{\partial E} D(E) E \tau dE, \tag{2.1.31}
$$

$$
L_{12} = -\frac{2q}{3mT} \int_{E=0}^{\infty} \frac{\partial f_0}{\partial E} D(E) E (E-\mu) \tau dE, \tag{2.1.32}
$$

$$
L_{21} = T L_{12}, \tag{2.1.33}
$$

$$
L_{22} = -\frac{2q}{3mT} \int_{E=0}^{\infty} \frac{\partial f_0}{\partial E} D(E) E (E-\mu)^2 \tau dE, \tag{2.1.34}
$$

The equations have now been set up to derive each of the different transport equations that are more familiar. To derive the different equations such as electrical conductivity, Seebeck coefficient and carrier concentration some basic initial conditions must be used.

2.1.1 Electrical Conductivity

The electrical conductivity is defined as a measure of the ability of a given substance to conduct electric current, equal to the reciprocal of the resistivity of the material.

To derive the conductivity from the Boltzmann transport equation, equation 2.1.28 is simplified using intial conditions for conductivity: no temperature gradient and no carrier concentration gradient. That is $\frac{dT}{dX} = 0$ and $\frac{d\mu}{dX} = 0$, and the equation then becomes

$$J_x = L_{11}(-\frac{1}{q}\frac{d\Phi}{dX}) = L_{11}(-\frac{1}{q}\frac{d\mu}{dX} + E_x) = L_{11}E_x. \tag{2.1.35}$$

From Ohm's law in basic electromagnetic theory [11], the charge density is equal to the conductivity times the electric field

$$\vec{J} = \sigma\vec{\mathcal{E}}. \tag{2.1.36}$$

Solving for σ produces

$$\sigma = \frac{J_x}{E_x} = L_{11} = -\frac{2q^2}{3m}\int_{E=0}^{\infty}\frac{\partial f_0}{\partial E}D(E)E\tau dE. \tag{2.1.37}$$

The partial derivative with respect to energy is non-zero only when the energy is close to the chemical potential

$$\frac{\partial f_0}{\partial E} = \delta(E-\mu), \tag{2.1.38}$$

So that

$$-\frac{2q^2}{3m}\int_{E=0}^{\infty}\delta(E-\mu)D(E)E\tau dE = \frac{2q^2}{3m}D(E)\mu\tau\Big|_{E=\mu} = \frac{2q^2}{3m}D_F\mu\tau_F. \tag{2.1.39}$$

τ_F is the scattering mean free time of Fermi electrons. τ_F is an electron's energy level near that of the Fermi energy. The chemical potential can be reduced to just the kinetic energy with the Fermi velocity. The Fermi level, also called the chemical potential, is equivalent

to the Fermi energy at T=0. Equation 2.1.39 can then be reduced using $\mu = E_F = \frac{1}{2}mv_F^2$, where v_F is the Fermi velocity, to give

$$\sigma = \frac{q^2}{3} D_F v_F^2 \tau_F. \tag{2.1.40}$$

The conductivity can be simplified more if the Fermi density D_F is replaced by the carrier concentration

$$\begin{aligned} n &= \int_{E=0}^{\infty} f_0(E) D(E) dE = \int_{E=0}^{\infty} f_0(E, T=0) D(E) dE = \int_{E=0}^{E_F} D(E) dE \\ &= \int_{E=0}^{E_F} \frac{1}{2\pi^2} \left(\frac{2m}{\hbar^2}\right)^{2/3} E^{1/2} dE = \frac{1}{3\pi^2} \left(\frac{2m}{\hbar^2}\right)^{2/3} E_F^{3/2} = \frac{2}{3} D_F E_F \approx \frac{2}{3} D_F \mu. \end{aligned} \tag{2.1.41}$$

Equation 2.1.39 and 2.1.41 can be combined to form the familiar form of the electrical conductivity

$$\sigma = \frac{q^2}{m} n \tau_F \tag{2.1.42}$$

2.1.2 Weidemann-Franz Law

The Wiedemann-Franz Law relates the electrical conductivity to the electrical component of the thermal conductivity. Assuming a mobility of

$$\mu_e = \frac{q}{m} \tau_F, \tag{2.1.43}$$

then with equation 2.1.42 the conductivity in terms of mobility is easily calculated to be

$$\sigma = nq\mu_e. \tag{2.1.44}$$

Combining electrical conductivity and thermal conductivity k_e (derived from the Boltzmann transport equation in Arabshahi [9]):

$$\frac{k_e}{\sigma} = \frac{\frac{1}{3}{\upsilon_F}^2 \tau_F C_e}{\frac{e^2}{m} n \tau_F} = \frac{m C_e {\upsilon_F}^2}{3ne^2}. \tag{2.1.45}$$

Here C_e is the electron specific heat obtained from the derivation of thermal conductivity transport equation:

$$C_e = \frac{1}{2}\pi^2 n k_B T / T_F = \frac{\frac{1}{2}\pi^2 n k_B T}{\frac{m{v_F}^2}{2k_B}} = \frac{\pi^2 n {k_B}^2 T}{m{v_F}^2}. \tag{2.1.46}$$

If the previous two equations are combined then the ratio of thermal to electrical conductivity is reduced to

$$\frac{k_e}{\sigma} = \frac{m{v_F}^2}{3ne^2}\frac{\pi^2 n {k_B}^2 T}{m{v_F}^2} = \frac{\pi^2 {k_B}^2 T}{3e^2}. \tag{2.1.47}$$

The Lorentz number is now defined to be

$$L = \frac{\pi^2 {k_B}^2}{3e^2} = 2.45 \times 10^{-8} (W\Omega/K^2), \tag{2.1.48}$$

and finally the Wiedemann-Franz law is obtained:

$$\frac{k_e}{\sigma} = LT. \tag{2.1.49}$$

2.1.3 Seebeck Effect

Unlike the case for conductivity, calculating the Seebeck coefficient requires a non-zero temperature gradient. It is defined as the measure of the magnitude of an induced thermoelectric

voltage in response to a temperature difference across that material. This temperature gradient is assumed to be along the X-axis of the sample. In this set up a voltage can be measured across the sample caused by the temperature gradient. Since there is no applied voltage, the charge flux is zero, $J_x = 0$, and

$$J_x = L_{11}(-\frac{1}{q}\frac{d\Phi}{dX}) + L_{12}(-\frac{dT}{dX}) = 0. \tag{2.1.50}$$

Accordingly, the change in electric potential divided by the temperature gradient is,

$$\frac{\frac{d\Phi}{dX}}{\frac{dT}{dX}} = -\frac{qL_{12}}{L_{11}}. \tag{2.1.51}$$

The voltage across the sample is $\nabla V = \nabla\Phi/q = \nabla(\mu + q\phi)$ and $dV = d\Phi/q$, and the Seebeck coefficient is

$$\begin{aligned} S = \frac{\frac{dV}{dX}}{\frac{dT}{dX}} = -\frac{1}{q}\frac{\frac{d\Phi}{dX}}{\frac{dT}{dX}} = \frac{L_{12}}{L_{11}} = \frac{1}{qT}\left(\frac{\int\limits_{E=0}^{\infty}\frac{\partial f_0}{\partial E}D(E)E(E-\mu)\tau dE}{\int\limits_{E=0}^{\infty}\frac{\partial f_0}{\partial E}D(E)E\tau dE}\right) \\ = \frac{1}{qT}\left(\mu - \frac{\int\limits_{E=0}^{\infty}\frac{\partial f_0}{\partial E}D(E)E^2\tau dE}{\int\limits_{E=0}^{\infty}\frac{\partial f_0}{\partial E}D(E)E\tau dE}\right). \end{aligned} \tag{2.1.52}$$

For the density of states of a solid, the free-electron density of states can be applied to describe the functions in the conduction and valence bands. [12] That is,

$$D(E) = \frac{\Omega(2m)^{3/2}}{2\pi^2\hbar^3}E^{1/2}, \tag{2.1.53}$$

where Ω is the volume.

To proceed further the relaxation time τ must be defined. τ depends on the energy of electrons according to a simple power law

$$\tau = \tau_0 E^r, \tag{2.1.54}$$

where r is a constant whose value depends on the types of scattering mechanisms involved. τ_0 is a constant that is independent of energy. r can have values such as $-1/2$ for acoustical phonon scattering or 0 for neutral impurity scattering.

Combining the relaxation time definition and the density of states with the Seebeck coefficient equation yields

$$S = \frac{1}{qT}\left(\mu - \frac{\int\limits_{E=0}^{\infty} \frac{\partial f_0}{\partial E} D(E) E^2 \tau dE}{\int\limits_{E=0}^{\infty} \frac{\partial f_0}{\partial E} D(E) E \tau dE}\right) = \frac{1}{qT}\left(\mu - \frac{\int\limits_{E=0}^{\infty} \frac{\partial f_0}{\partial E} E^{2+r+1/2} \tau dE}{\int\limits_{E=0}^{\infty} \frac{\partial f_0}{\partial E} E^{1+r+1/2} \tau dE}\right). \tag{2.1.55}$$

The integrals of equation 2.1.55 can be simplified to

$$\int\limits_{E=0}^{\infty} \frac{\partial f_0}{\partial E} E^r dE = f_0 E^r \Big|_0^{\infty} - r \int\limits_{E=0}^{\infty} f_0 E^{r-1} dE = -r \int\limits_{E=0}^{\infty} f_0 E^{r-1} dE. \tag{2.1.56}$$

Equation 2.1.55 now reduces to

$$S = \frac{1}{qT}\left(\mu - \frac{(r+5/2) \int\limits_{E=0}^{\infty} f_0 E^{r+3/2} \tau dE}{(r+3/2) \int\limits_{E=0}^{\infty} f_0 E^{r+1/2} \tau dE}\right). \tag{2.1.57}$$

This can be simplified by changing the energy E to the reduced energy $E = \zeta k_B T$

$$\int\limits_{E=0}^{\infty} f_0(E,\mu) E^n dE = (k_B T)^{n+1} \int\limits_{0}^{\infty} f_0(E,\zeta) \zeta^n d\zeta = (k_B T)^{n+1} F_n(\eta), \tag{2.1.58}$$

where the Fermi-Dirac integral is

$$F_n(\eta) = \int_0^\infty f_0(\zeta, \eta)\zeta^n d\zeta. \tag{2.1.59}$$

The values for this integral can be found in Appendix A. This equation will be used to measure the relation between the Seebeck coefficient and carrier concentration. Fermi-Dirac integrals can be calculated with the help of built-in functions in Mathematica or MATLAB, but these tabulated values work well, too. The rest of the derivation will be for the purpose of calculating via computer. The nearly final form of the Seebeck coefficient is

$$S = -\frac{k_B}{q}\left(\eta - \frac{(r+\frac{5}{2})F_{r+\frac{5}{2}}}{(r+\frac{3}{2})F_{r+\frac{5}{2}}}\right). \tag{2.1.60}$$

For a non-degenerate semiconductor the chemical potential is located a distance from the conduction or valence band larger than $3k_BT$. If the distance is larger than that of the reduced energy ζ minus the location of the Fermi level with respect to the conduction band η is greater than three ($\zeta - \eta > 3$), the integral then becomes

$$\begin{aligned} F_n(\eta) &= \int_0^\infty f_0(\zeta, \eta)\zeta^n d\zeta = \int_0^\infty \frac{1}{exp(\zeta - \eta) + 1}\zeta^n d\zeta = \int_0^\infty \frac{1}{exp(\zeta - \eta)}\zeta^n d\zeta \\ &= exp(\eta)\int_0^\infty exp(-\zeta)\zeta^n d\zeta = exp(\eta)\Gamma(n+1), \end{aligned} \tag{2.1.61}$$

where the gamma function, a useful tool for integration of problems with an exponential function and a linear function, is

$$\Gamma(n+1) = \int_0^\infty exp(-\zeta)\zeta^n d\zeta = n\Gamma(n). \tag{2.1.62}$$

Substituting in the Gamma function the Seebeck coefficient is given by

$$S = -\frac{k_B}{q}\left(\eta - \frac{(r+\frac{5}{2})exp(\eta)\Gamma(r+\frac{5}{2})}{(r+\frac{3}{2})exp(\eta)\Gamma(r+\frac{3}{2})}\right). \tag{2.1.63}$$

2.2 Hall Effect

Beginning again with the Boltzmann transport equation the Hall coefficient R_H may be derived. The Hall effect derivation follows Harrison, Solid State Theory.[10] Start with the basic relationship

$$\vec{F} \cdot \frac{1}{\hbar}\nabla_k f(\vec{k}) = \frac{\partial f}{\partial t}. \tag{2.2.1}$$

In this case the force is due to both the applied electrical and magnetic fields, $\vec{F}$ here is the Lorentz force,

$$\vec{F} = q(\vec{\mathcal{E}} + \vec{v} \times \vec{B}), \tag{2.2.2}$$

so that

$$q(\vec{\mathcal{E}} + \vec{v} \times \vec{B}) \cdot \frac{1}{\hbar}\nabla_k f(\vec{k}) = \frac{\partial f}{\partial t}. \tag{2.2.3}$$

Assuming the relaxation time approximation τ equation 2.2.3 becomes

$$\left(q(\vec{\mathcal{E}} + \vec{v} \times \vec{B})\right) \cdot \left(\frac{1}{\hbar}\nabla_k f(\vec{k})\right) = \frac{f - f_0}{\tau} \tag{2.2.4}$$

and

$$\frac{\partial f_0}{\partial E}\vec{v} \cdot \left(-q\vec{\mathcal{E}} - q\vec{v} \times \vec{B}\right) + \frac{\partial f_1}{\partial \vec{p}} \cdot \left(-q\vec{\mathcal{E}} - q\vec{v} \times \vec{B}\right) + \frac{f_1}{\tau} = 0 \tag{2.2.5}$$

Now the equation 2.2.5 can be simplified using the fact that the divergence of the curl is zero $\vec{v} \cdot (\vec{v} \times \vec{B}) = 0$ and that $\frac{\partial f_1}{\partial \vec{p}} \cdot (-q\vec{\mathcal{E}})$ is a second order term and can be neglected.

$$-q\frac{\partial f_0}{\partial E}\vec{v} \cdot \vec{\mathcal{E}} - q\frac{\partial f_1}{\partial \vec{p}} \cdot (\vec{v} \times \vec{B}) + \frac{f_1}{\tau} = 0. \tag{2.2.6}$$

Solving for the first-order term f_1 is impossible, but if the equation is analysed, it can be noted that when considering a steady state problem it is possible to solve for the first-order term. In a steady state problem, the Boltzmann equation is reduced to

$$f_1 = \frac{\partial f_0}{\partial \vec{p}} \cdot \tau \vec{F}. \tag{2.2.7}$$

Noting that $\frac{\partial f_0}{\partial \vec{p}} = \frac{\partial f_0}{\partial E}\frac{\partial E}{\partial \vec{p}} = \frac{\partial f_0}{\partial E}\vec{v}$ from equation 2.1.5 makes Eq. 2.2.7

$$f_1 = \tau\bigg(- \frac{\partial f_0}{\partial E}\bigg)\vec{v} \cdot \vec{F}. \tag{2.2.8}$$

Reverting back to the original problem, equation 2.2.6., the first partial term is similar to that of the steady state problem, while the second partial term is the magnetic field term and is there to rotate the distribution. Equation 2.2.7 can be substituted into 2.2.6 if the electric field is replaced by a general vector $\vec{G}$ the distribution function is

$$f_1 = q\tau \frac{\partial f_0}{\partial E}\vec{v} \cdot \vec{G}. \tag{2.2.9}$$

This is able to help solve the first partial term but the derivative of f_1 with respect to momentum, $\vec{p}$, for the second partial term is

$$\frac{\partial f_1}{\partial \vec{p}} = q\tau\bigg[\frac{\vec{G}}{m}\frac{\partial f_0}{\partial E} + \frac{\partial^2 f_0}{\partial E^2}(\vec{v}\cdot\vec{G})\vec{v}\bigg]. \tag{2.2.10}$$

Equation 2.2.10 can be combined with 2.2.6 to form

$$\begin{aligned} 0 = &- q\frac{\partial f_0}{\partial E}\vec{v}\cdot\vec{\mathcal{E}} - q^2\tau\bigg[\frac{\vec{G}}{m}\frac{\partial f_0}{\partial E} + \frac{\partial^2 f_0}{\partial E^2}(\vec{v}\cdot\vec{G})\vec{v}\bigg]\cdot(\vec{v}\times\vec{B}) + q\frac{\partial f_0}{\partial E}\vec{v}\cdot\vec{G} \\ &= -q\frac{\partial f_0}{\partial E}\vec{v}\cdot\vec{\mathcal{E}} - q^2\tau\bigg[\frac{\vec{G}}{m}\frac{\partial f_0}{\partial E}\bigg]\cdot(\vec{v}\times\vec{B}) + q\frac{\partial f_0}{\partial E}\vec{v}\cdot\vec{G}. \end{aligned} \tag{2.2.11}$$

The second order partial derivative term goes to zero because it results in a divergence of a curl. Also each of the $\frac{\partial f_0}{\partial E}$ cam ne dropped out of the equation along with the charge, q and τ tp equal

$$0 = -\vec{v} \cdot \vec{\mathcal{E}} - \frac{q\tau}{m}\vec{G} \cdot (\vec{v} \times \vec{B}) + \vec{v} \cdot \vec{G}. \tag{2.2.12}$$

The equation above can be rearranged to yield

$$0 = \vec{v} \cdot \left(\vec{\mathcal{E}} + \frac{q\tau}{m}\vec{G} \times \vec{B} - \vec{G}\right). \tag{2.2.13}$$

For this to be true, the total electric field would have to be

$$\vec{\mathcal{E}} = \vec{G} - \frac{q\tau}{m}(\vec{G} \times \vec{B}). \tag{2.2.14}$$

Now when the magnetic field is non-existent only the first term is left so $\vec{\mathcal{E}} = \vec{G}$. Ohm's law, $\vec{J} = \sigma\vec{E}$, allows the identification of the vector $\vec{G}$ as $\vec{G} = \vec{J}/\sigma$. Substituting yields

$$\vec{\mathcal{E}} = \frac{J}{\sigma} + \frac{q\tau}{m\sigma}(\vec{B} \times \vec{J}), \tag{2.2.15}$$

this shows that in the presence of a magnetic field, the electric field has two components, one in the direction of $\vec{J}$ and one in the direction of $\vec{B} \times \vec{J}$. Using Fig. 1.2,

$$\mathcal{E}_x = \frac{J_x}{\sigma} \tag{2.2.16}$$

and

$$\mathcal{E}_y = \frac{q\tau}{m\sigma}B_z J_x \tag{2.2.17}$$

or

$$\frac{\mathcal{E}_y}{B_z J_x} = \frac{q\tau}{m\sigma} = R_H = \frac{\mu_H}{\sigma} \tag{2.2.18}$$

with the mobility identified as $\mu_H = \frac{q\tau}{m}$.

This is the Hall coefficient, a constant that is able to determine the carrier type of the material, whether it is n-type or p-type based on the sign of the charge term, q, $(q = -e)$ for n-type or electrons and $(q = +e)$ for p-type or holes. n is the carrier concentration of the material.

$$n = \frac{1}{|R_H|e} \tag{2.2.19}$$

2.3 Scattering Parameter "r"

The scattering parameter, r, was talked about in section 2.1.2, but was glossed over. This parameter is a number of either -1/2, 0, 1/2, 3/2 that defines the type of scattering that occurs in a solid. The values focused in this paper is 0 and -1/2 corresponding to acoustic phonon scattering (-1/2) and neutral impurity scattering (0). [13] These equations are derived above the Seebeck coefficient section and the electrical conductivity section.

$$S = -\frac{k_B}{q}\left(\eta - \frac{(r+\frac{5}{2})F_{r+\frac{5}{2}}}{(r+\frac{3}{2})F_{r+\frac{5}{2}}}\right) \tag{2.3.1}$$

$$n = \frac{N_V}{2\pi^2}\left(\frac{2k_B T m_d}{\hbar^2}\right)^{3/2} F_{1/2}(\zeta^*) \tag{2.3.2}$$

Equation 2.3.2 is the carrier concentration from the conductivity section. Here N_v is the number of valleys in the semiconductor and the equation is easily defined when the integral in Eq. 2.1.41 is replaced by the Fermi-integral. Then Eq. 2.3.2 is easily calculated.

Chapter 3

EXPERIMENTAL SETUP

The experiments presented here are performed to accurately characterize newly synthesized thermoelectric compounds. We use instruments both built and acquired to measure the properties of carrier concentration, Seebeck coefficient, mobility, and conductivity. Resistivity and the hall coefficient are obtained.

There are two main experimental set ups to be discussed along with the appropriate guidelines needed to perform them. First is the Hall effect apparatus built to measure the carrier concentration, mobility, and conductivity. The second machine used for characterization is the ULVAC ZEM3. The ZEM3 is able to measure resistivity, Seebeck coefficient, power factor and figure of merit. Among all these properties we only need the Seebeck coefficient and the conductivity from the Hall measurement for characterizing the electrical components of a thermoelectric material.

3.1 Samples

There are several stages to the sample synthesis and preparation for measurement in the ZEM-3 and Hall effect instruments. First a sample is synthesized as a powder, then the powder form is put into a laboratory hot press. After the powder is solidified to a certain hardness, the solid sample is then cut into rectangular blocks approximately 3mm x 3mm

x 10mm. These blocks are the basic sample dimensions used for measurements in both the ZEM and Hall effect devices.

3.2 Hall Effect

3.2.1 Geometry

When measuring the Hall effect two sample geometries are often used, the Hall bar and the Van der Pauw geometries. Each has advantages and disadvantages. The most common geometry for research is the Hall bar geometry shown in Fig. 3.1. The Hall bar geometry uses a long narrow rectangular sample, with the simplest lead placement being a 4 point contact. In the 4-contact set up there are two leads passing a current across the long axis of the sample, while two voltage leads are placed on the side of the sample directly across from one another, as accurately as possible.

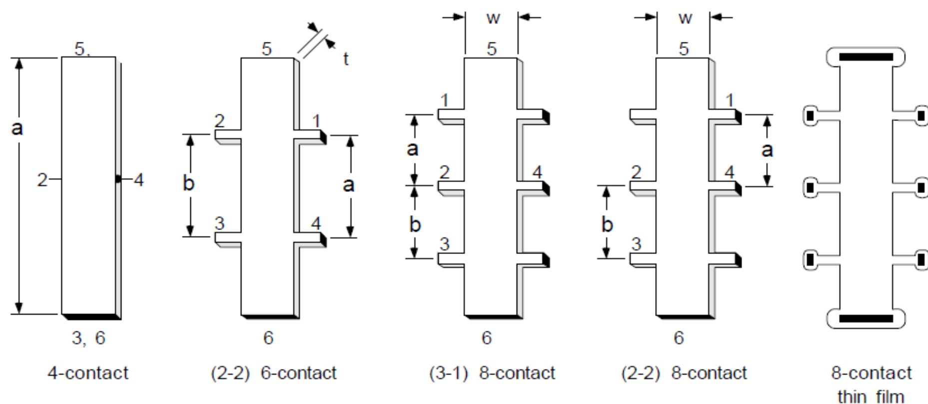

FIGURE 3.1: Hall effect geometry for a rectangular bar sample. [14]

For calculating the Hall coefficient R_H after the data have been collected with the Hall bar geometry, for the 4 contact bar geometry

$$R_H = \frac{tV_{24}}{I_{56}B}, \tag{3.2.1}$$

Here the V_{24} means that the voltage is read from points 2 and 4 from Figure 3.1, while at the same time current is passing through points 5 and 6, I_{56}. While the 4 contact bar is by far the easiest to implement in any system, it is not the most accurate and can have trouble in determining resistivity and whether or not the sample is inhomogeneous or anisotropic. The 6 contact and 8 contact bar are suited for measuring these values. For the 6 point the Hall coefficient is

$$R_{H,34} = \frac{t(V_+ - V_-)_{34}}{eI_{56}(B_+ - B_-)} \tag{3.2.2}$$

$$R_{H,12} = \frac{t(V_+ - V_-)_{12}}{eI_{56}(B_+ - B_-)} \tag{3.2.3}$$

Equations 3.2.2 and 3.2.3 are then averaged and the real value of the Hall coefficient is determined.

$$R_H = \frac{R_{H,34} + R_{H,12}}{2}, \tag{3.2.4}$$

If the values of $R_{H,34}$ and $R_{H,12}$ differ by more than 10% then the sample is in fact anisotropic. Equations 3.2.2 and 3.2.3 can be adapted for the 8 contact bar with an addition of $R_{H,56}$.[14]

We use a non-standard 5 contact geometry for measure the Hall voltage and resistivity. Equation 3.2.1 is used to measure the Hall coefficient. A 5 contact geometry is similar to the 4 contact geometry except for the fact that with 5 points of contact, a resistivity can also be measured. Fig 3.2 shows the wire configuration.

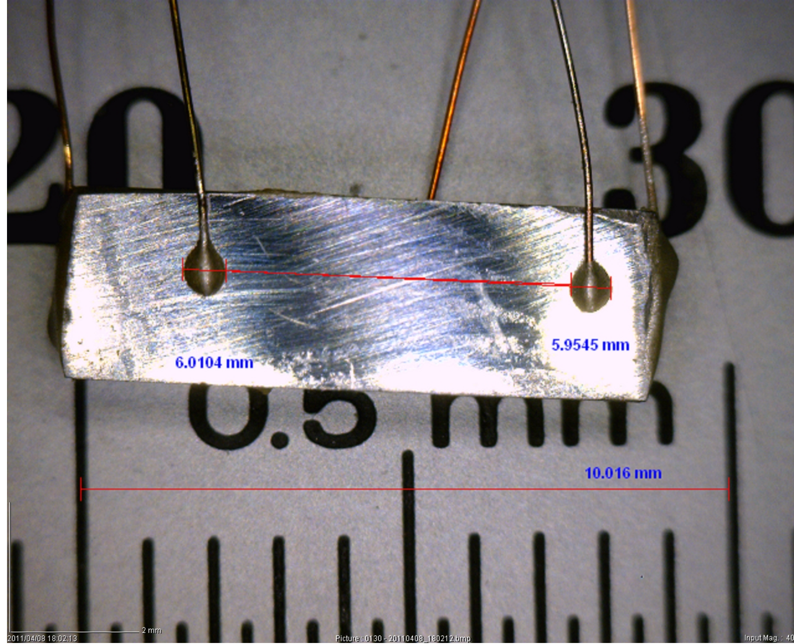

FIGURE 3.2: Sample with 5 contacts and silver paste contacts.

The Van der Pauw geometry shown in Fig. 3.2 is the most popular in industry due to the fact that the measurements require fewer geometrical constraints. If the sample has a uniform thickness, homogeneity, and contains no holes in it, then the Van der Pauw method works. Nearly any shape can be used. Drawback to the Van der Pauw method is the fact that because of the fact that the contacts are not on the circumference of the sample, it is impossible to accurately measure magnetoresistance and the current flow is not as precise as that of the Hall bar geometry. Methods can be used to reduce the error caused if the contacts are of finite size and not sufficiently close to the circumference, such as using a "clover" leaf design shown in Figure 3.3.

The Van der Pauw calculations are as follows, where each field is a sum of the positive and negative magnetic field values:

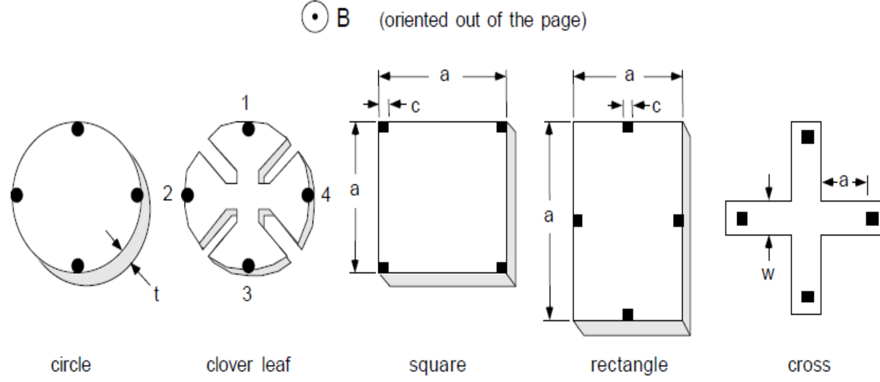

FIGURE 3.3: Hall effect geometry for the Van der Pauw method.[14]

$$
\begin{aligned}
V_{13} &= V_{13,P} - V_{13,N} \\
V_{24} &= V_{24,P} - V_{24,N} \\
V_{31} &= V_{31,P} - V_{31,N} \\
V_{42} &= V_{42,P} - V_{42,N}
\end{aligned}
\tag{3.2.5}
$$

Once again voltage is read from the two points labelled but the current is passed from the two points that aren't labelled so for V_{13} the current is I_{24}. These voltages are the voltage measured when the magnetic field is in the positive direction minus the voltage measure when the field is in the negative direction. There must be four voltage measurements for the Van der Pauw to ensure

$$V_H = \frac{V_{13} + V_{24} + V_{31} + V_{42}}{8} \tag{3.2.6}$$

And as before the Hall coefficient is able to be calculated with the Hall voltage.

$$R_H = \frac{tV_H}{BI} \tag{3.2.7}$$

Because of the layout of the voltages and currents measured, the time required to take the measurement for the Van der Pauw method is increased when compared to the Hall bar. This is because of the switching required to pass the current and measure the voltage for 8 different orientations with positive and negative field values.

3.2.2 Hall Equipment

FIGURE 3.4: Hall effect system designed, built and programmed for our lab.

The equipment used here is pieced together for our specific purposes, which include: Lake Shore 455 DSP Gaussmeter, a Lake Shore 370 AC Resistance Bridge, a Lake Shore 3708 Pre-Amplifier Scanner, a GMW Electromagnet, and a GMW System 8500 Magnet Power Supply. The Lake Shore 370 AC Resistance Bridge was chosen because of the range of sample resistance runs from 2mΩ to 2MΩ.

All instruments are connected to a computer via a General Purpose Interface Bus, GPIB. GPIB is a standard among most automatic test instruments allowing easy to use programs, such as Labview, for programming the instruments.

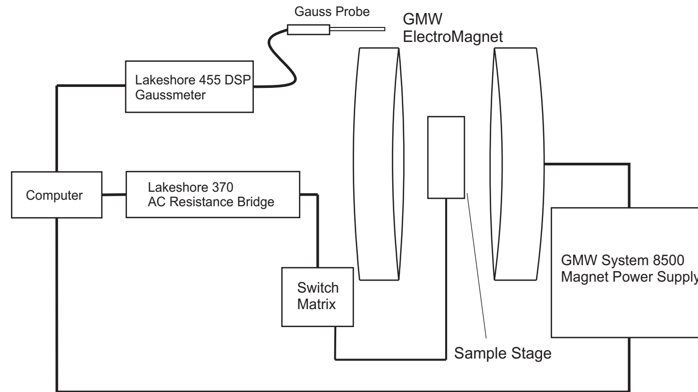

FIGURE 3.5: Basic elements in a working setup to measure the Hall effect.

The Lake Shore 370 AC Resistance Bridge is the main instrument of the Hall effect apparatus. This device has two modes: voltage excitation mode and current excitation mode. For measuring the Hall effect, the current must be controlled so the latter mode is used. This mode is able to pass a current from 3.16 pA (pico-Amps) to 31.6 mA (milli-Amps), with 21 preset levels in between. When in current excitation mode, each amperage has associated voltages that can be measured. The voltage being measured is determined by a range of resistances. For example, when 10 mA is set, you then simultaneously set the resistance range to fine tune the voltage that is being measured. Since the current is a preset value, the instrument displays values of resistance instead of voltage even though its the voltage that really is being measured. Ohm's law, $V = IR$, will provide the measured voltage. These preset amperage and resistance ranges are found in Appendix D.

The Lake Shore 3708 Scanner is an subsidiary unit for the Lake Shore 370. The 3708 is an eight channel pre-amplifier scanner where one side interfaces with the Lake Shore to provide channels to measure and scan while the other end is able to have active connections to and from the samples being measured. This scanner card is able to provide eight simultaneous attached connections to the material being measured. This is done by "nulling" out the inactive channels allowing for clear and precise measurement without interference from different channel configurations.

The Lake Shore 455 DSP Gaussmeter is part of the system used solely for measuring accurate readings of the magnetic field. In figure 3.3 the gaussmeter probe or gauss probe should go in between the poles of the GMW magnet. The maximum and minimum fields able to be read by the High Sensitivity probe is listed in Appendix A.

The final instruments needed are the GMW magnet and GMW power supply. The magnet has a maximum field output of 1.2 T when the poles are at a distance of 7 cm apart. The poles of the magnet are 10 cm in diameter.

The magnetic field is a DC field. The current to the sample is AC. The Lake Shore 370 produces a precision AC current (13 Hz) and measures a potential difference. It typically reports the value as a resistance or V/I.

3.2.3 Samples in Hall Effect Apparatus

Once ohmic contact annealing took place the sample was moved to the apparatus for measurement. Sample leads are soldered to the pre-existing wires from the resistance bridge and mounted firmly on the sample stage and the stage placed within the uniform magnetic field. The sample is oriented with the current being perpendicular to the magnetic field which produces a voltage that is perpendicular to both current and magnetic field. The Lake Shore 370 performs the switching between resistivity and hall measurements.

Once the sample is within the magnetic field, data is taken while sweeping the field from -0.5 Tesla to 0.5 Tesla. Positive and minus values of the magnetic field must be taken in order to cancel out any extra voltage later from the leads being misaligned. The instruments and data taken are controlled by National Instruments Labview programming and provides seamless integration of the different instruments.

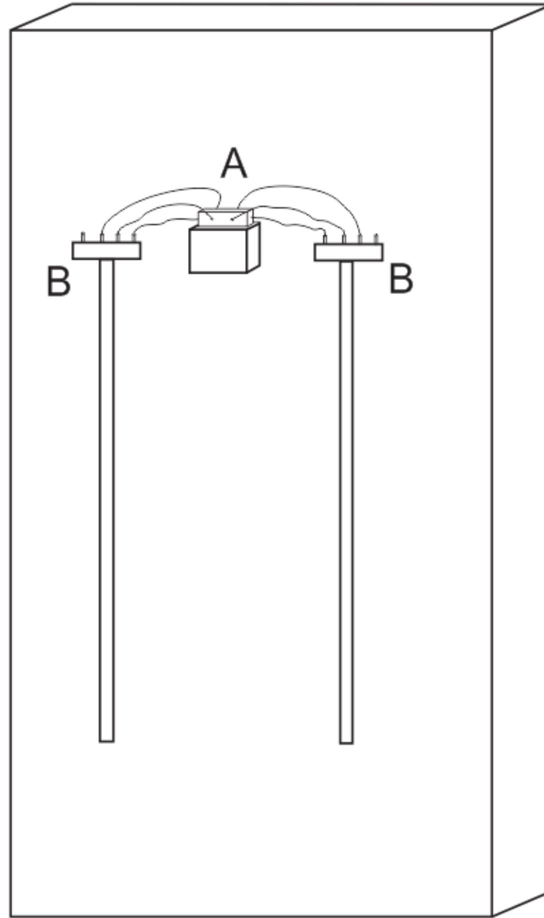

FIGURE 3.6: Sample stage to be placed within the magnetic field. A is the sample being measured. B is the wiring harness for cables that are connecting the 6 point Hall measurement to the Lake Shore 3708 Scanner

3.2.4 Ohmic Contact Fabrication

The process of measuring the Hall effect starts with applying reliable and uniform ohmic contacts to the material. One of the most common methods is to use a silver paste, PELCO High Performance Silver Paste, to adhere five ohmic contacts to the sample. The Silver Paste is a one part epoxy used for temperature ranges from cryogenic to 1200K. The PELCO High Performance Silver Paste was applied under a microscope to ensure a contact as small as possible to have minimal ohmic dependence.

After the contacts are set in place they are annealed at 300K for two hours and then at 360K for two more hours. These samples were prepared for the Hall Bar geometry with a five point contact to accurately measure the Hall voltage and resistivity simultaneously. All measurements were made at 300K.

3.2.5 Hall Data Analysis

Data from the Lake Shore 370 is in an un-averaged raw form. The first calculation is averaged over all values to prevent large variances. This is done in Labview.

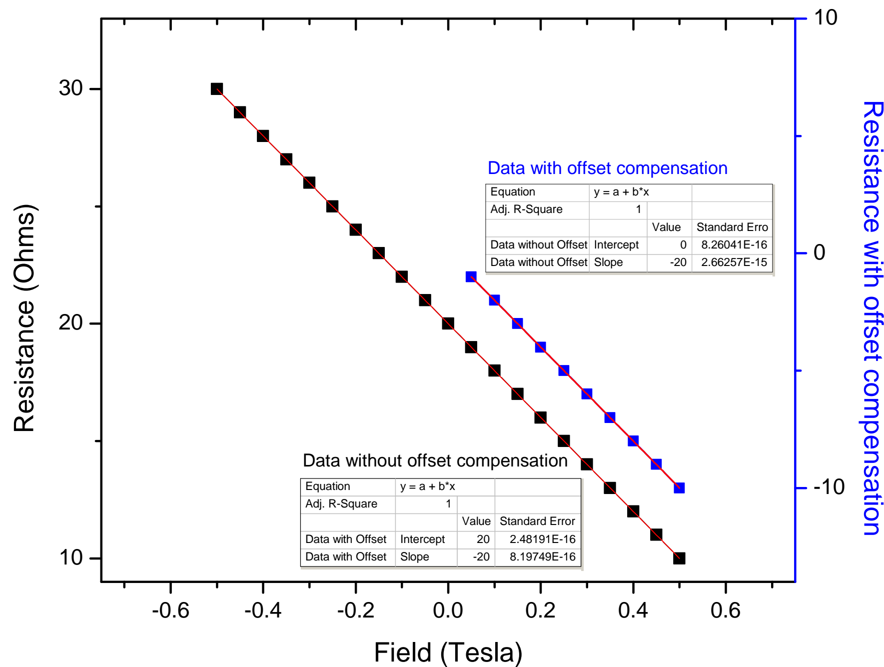

FIGURE 3.7: Example data for adjustment of the offset voltage that occurs with misaligned voltage wires.

Data is tabulated using Origin 8.0. Generally the initial data will contain an offset voltage caused by imperfect wire placement on the sample. This can be corrected using the zero field voltage measured when the field was swept from -0.5 Tesla to 0.5 Tesla. This results in the voltages passing through zero when the magnetic field is turned off. This effect is illustrated in Figure 3.5. When the leads are misaligned the Hall voltage is then

$$V_H = \frac{R_H I B_z}{d} + V_0. \quad (3.2.8)$$

When the voltage is plotted versus the magnetic field, a straight line should be produced. Noise from vibrations, grounding problems, and the magnetic field's uniformity being unstable can cause large variations in the values. If the data is plotted and it does not follow linear dependence then the sample could have a magneto-resistant properties or be magnetic.

In Figure 3.5 are two lines of data from a typical measurement. The offset compensation is the voltage found at 0.0 Tesla. Correcting the voltage provide an accurate measurement for the Hall effect without error from the wire placement. The slope of the line times the thickness will give the Hall coefficient $R_H = \frac{V_H d}{B_z I_x}$.

To ensure that the instruments were correctly calibrated, a stainless steel Standard Reference Material (SRM) was used to reproduce the resistivity measured by the National Bureau of Standards and National Institute of Standards and Technology (NIST). The stainless steel was SRM 1461 and a table of values can be found in Appendix G.

3.3 ZEM Equipment

For the Seebeck coefficient measurements, the ZEM-3 from ULVAC Technologies, Inc. was used. This instrument is able to measure the Seebeck coefficient and resistivity simultaneously. It can measure samples of length 6 mm to 22 mm in both rectangular prism and cylindrical shapes. For Bi_2Te_3 pure and nano-composite materials, 10 mm long prisms were used for the Seebeck measurement. The instrument is controlled via computer to automate measurement with temperature ranging from room temperature to $800°C$. Measurements are performed under an inert atmosphere of helium gas.

The Seebeck coefficient measurement uses a static DC method, while measuring the electrical resistance uses a standard four point method.

Bismuth has a melting point of $271.4°C$. In the ZEM-3, the Bi_2Te_3 pure and nano-composite materials were measured from room temperature to $150°C$ to ensure that no bismuth nano-particles would melt and possibly enter the Bi_2Te_3 matrix.

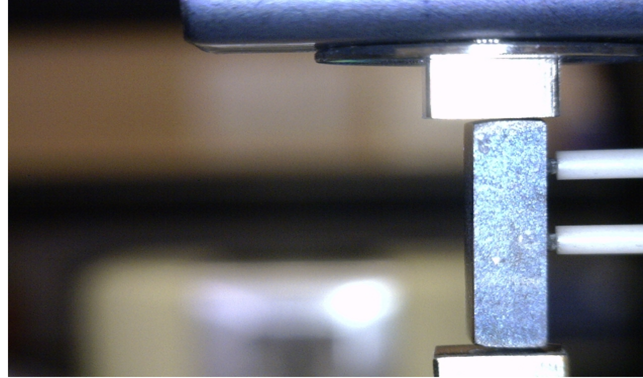

FIGURE 3.8: ZEM3 sample stage with probes in place.

In Figure 3.6 a sample is shown mounted in the ZEM3 with the temperature and current probes in place. The sample is held in place by pressure contacts on the top and bottom. A furnace is then brought into place and the sample is secured inside the furnace. A vacuum is produce and inert gas fills the chamber to ensure no contamination from the air. The probes measure the voltage when a current is passed through the sample and when the sample has a temperature gradient on its long axis. These two different voltages are the conductivity and the Seebeck coefficient respectively. The instrument is controlled via Labview.

Chapter 4

RESULTS

4.1 Structure of Bi_2Te_3/Bi Nanocomposite

Experimental results for electronic transport measurements discussed in Chapter 2 and 3 are described in this section. Results have been published in Advanced Energy Materials, "Enhancement in thermoelectric figure of merit in nano-structured Bi_2Te_3 with semimetal nanoinclusions".[13]

4.2 Electronic Transport Measurements

As listed in Table 4.1, eleven different samples were investigated. Varying fractions of Bi nanoparticles (0-7%) were dispersed into the Bi_2Te_3 matrix. In addition, off-stoichiometric $Bi_{2-x}Te_{3+x}$ was synthesized to produce nanostructured materials with different carrier concentration for comparison. Measurements of the Hall coefficient, resistivity, and the Seebeck coefficient were taken. Several different sample sets were made for more in depth comparison. In batch I of the bismuth telluride, we have a single sample of just the bismuth telluride matrix accompanied by two nanocomposite samples of 3% and 5% bismuth nano-inclusions.

Batch II consists of a similar grouping, but the percentage of bismuth nano-inclusions were increased to 5% and 7%. The third grouping in the table is the off-stoichiometric contributions with varying degrees of ratio between bismuth and tellurium but no nano-inclusions

Table 4.1: Table of Measured and Calculated Values

Sample Name	Hall Coefficient (cm^3/C) R_H	Resistivity $(\Omega \cdot cm)$ ρ	Carrier Concentration $(\times 10^{19}/cm^3)$ n	Carrier Mobility $(cm^2/V \cdot s)$ μ_e	Seebeck Coefficient $(\mu V/K)$ S
Bi_2Te_3 **- I**	-3.78×10^{-1}	5.20×10^{-3}	1.652	72.607	178
$Bi/Bi_2Te_3(3\%Bi\ NC)$	-2.92×10^{-1}	4.35×10^{-3}	2.653	54.044	167
$Bi/Bi_2Te_3(5\%Bi\ NC)$	-2.03×10^{-1}	2.76×10^{-3}	3.08	73.297	171
Bi/Bi_2Te_3 **- II**	-4.13×10^{-1}	1.96×10^{-3}	1.51	210.82	182
$Bi/Bi_2Te_3(5\%Bi\ NC)$	-1.12×10^{-1}	1.58×10^{-3}	5.571	70.955	138
$Bi/Bi_2Te_3(7\%Bi\ NC)$	-1.14×10^{-1}	1.44×10^{-3}	5.462	79.5	139
$Bi_{1.95}Te_{3.05}$	-2.88×10^{-1}	3.65×10^{-3}	2.169	78.755	159
$Bi_{1.85}Te_{3.15}$	-2.51×10^{-1}	2.67×10^{-3}	2.489	93.893	156
$Bi_{1.75}Te_{3.25}$	-1.83×10^{-1}	2.50×10^{-3}	3.415	73.084	150
$Bi_{1.95}Te_{3.05}(3\%Bi\ NC)$	-1.68×10^{-1}	2.63×10^{-3}	3.707	63.978	141
$Bi_{1.95}Te_{3.05}(5\%Bi\ NC)$	-1.48×10^{-1}	2.51×10^{-3}	4.213	59.031	126

are considered with the lower ratio bismuth to tellurium samples. Only two bismuth nano-inclusion percentages (3% and 5%) were included in the synthesis for the smallest change in ratio.

The Hall effect measurements show an increase in carrier concentration in the Bi/Bi_2Te_3 nanocomposite and $Bi_{2-x}Te_{3+x}$ samples (for 3%, 5%, and 7% Bi nano-inclusions) compared to the matrix phases. The carrier mobility of the 3%Bi/Bi_2Te_3 nanocomposite decreases compared to the matrix while it again increases for 5%Bi/Bi_2Te_3 nanocomposite.

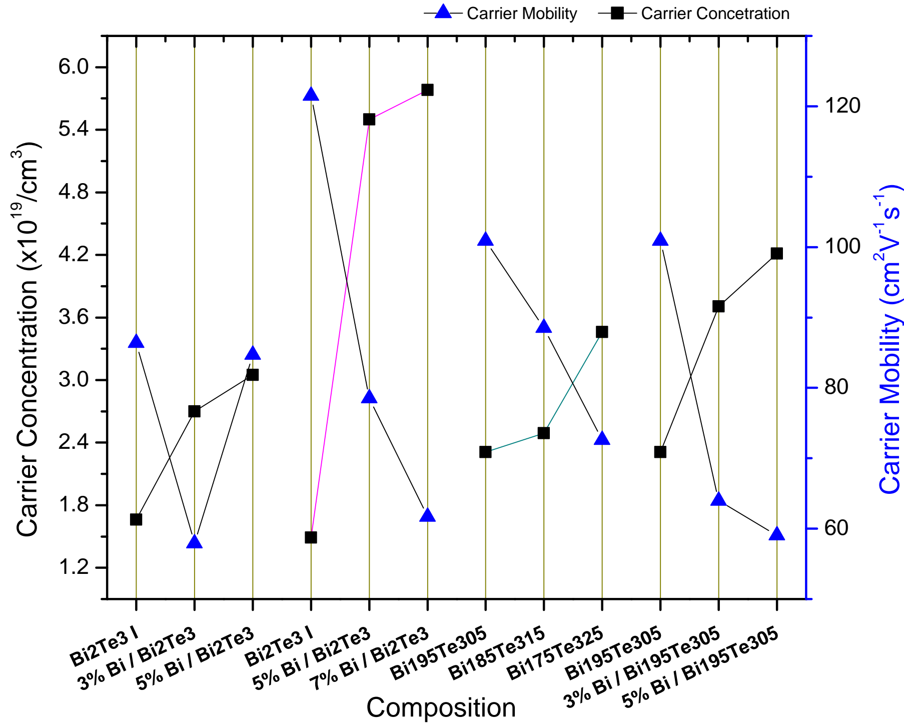

FIGURE 4.1: Carrier concentration / mobility vs. Composition. The points connected by a line are of the same set. We see a trend of increasing carrier concentration with a decrease in mobility based on the composition.

In Figure 4.1 the carrier concentration versus composition and carrier mobility versus composition is shown at room temperature (300K). It can be seen that with an increasing carrier concentration the carrier mobility decreases in agreement with equation 1.2.11. One anomaly exists in the data with the 5% bismuth telluride nanocomposite. It has a is slightly larger than the 3% bismuth telluride nanocomposite. This is explained by slight variations in ball-milling, manual mixing procedures, and hot-pressing conditions result in small deviations in stoichiometry and consequently deviations in electronic transport.

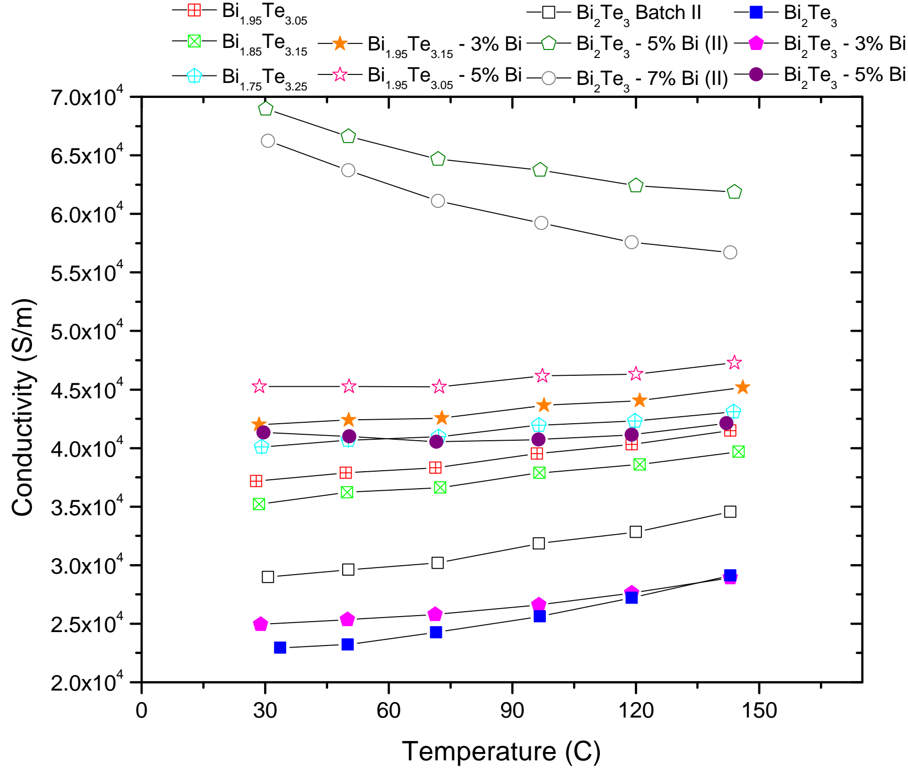

FIGURE 4.2: Plot of Conductivity vs. Temperature. Data was taken on the ZEM3.

The ratio of bismuth to tellurium in $Bi_{2-x}Te_{3+x}$ results in variation of the conductivity and Seebeck coefficient. When adding tellurium to the system, the electrical conductivity increases. In single crystal Bi_2Te_3 with no doping, the carrier type is p, but with this nano-structured stoichiometric compound Bi_2Te_3 it is measured as n-type. [15] Milling conditions and densification temperatures must be taken into account when studying electrical conductivity and the Seebeck coefficient of mechanically alloyed materials. When bismuth nano-inclusions are added to the Bi_2Te_3 the results show an increased carrier concentration and an increase in electrical conductivity when compared to the Bi_2Te_3 pure samples.

The conductivity in Fig. 4.2 shows that when Bi_2Te_3 has bismuth nano-inclusions the conductivity is increased. That is, for the 5% and 7% nano-composites, the conductivity doubled when compared to the base, while the 3% increased by a small margin and was similar to the base at high temperatures. In the off-stoichiometric with decreasing bismuth

concentration, the conductivity decreased and then increased, but all had a similar trend in temperature. The off-stoichiometric nano-composites also saw a similar effect as the Bi_2Te_3 nano-composites, with an increase in conductivity when bismuth nano-inclusions were incorporated.

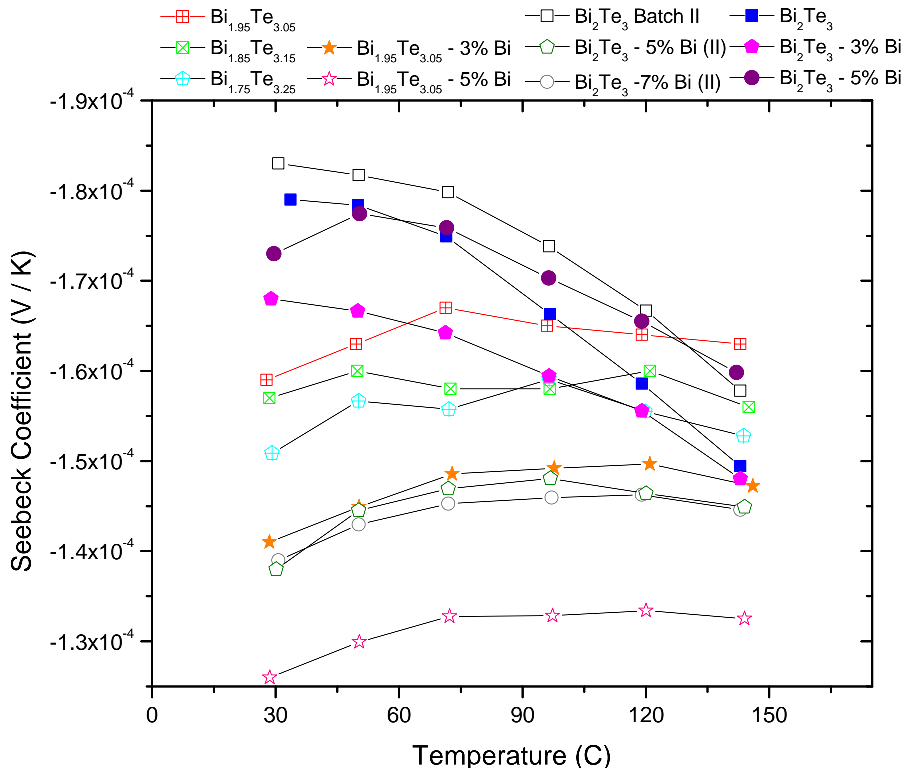

FIGURE 4.3: Plot of Seebeck Coefficient vs. Temperature.

Fig. 4.3 shows the Seebeck coefficient for the bismuth telluride nano-composites. Here the data shows that with an increase in bismuth nano-inclusions the Seebeck coefficient changes slightly but not as much as the conductivity. This can be attributed to the bismuth nano-inclusions increasing the conductivity but not affecting the Seebeck coefficient, meaning an overall higher ZT for a thermoelectric material.

4.3 Electron Filtering Results

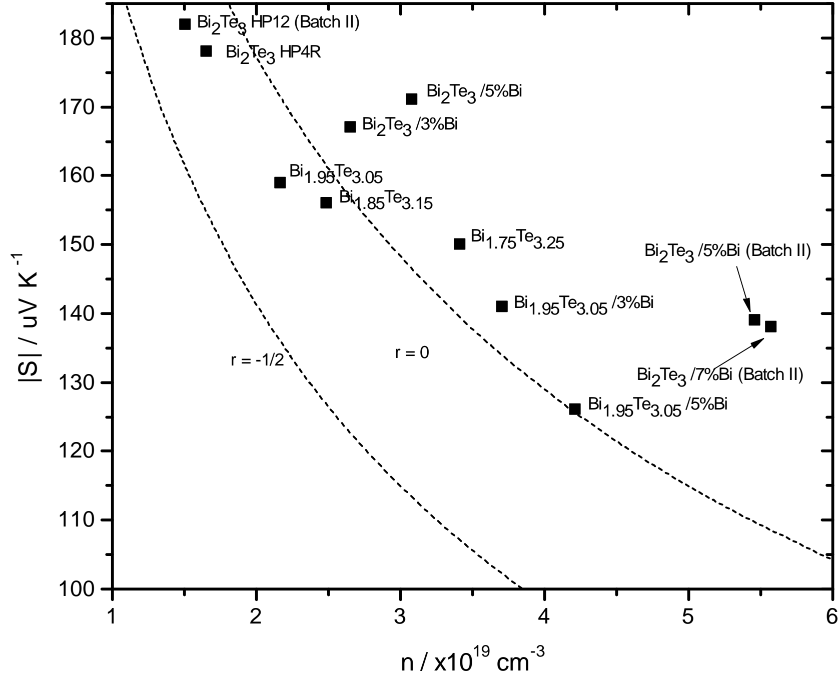

FIGURE 4.4: The Pisarenko plot of Seebeck coefficient vs. carrier concentration shows the dotted line is the prediction from basic transport theory of r=-1/2 and r=0, the trend of samples clearly show a dependence on some other type of scattering parameter.

The Pisarenko plot, Figure 4.4, is a relationship of carrier concentration n vs the Seebeck coefficient S and the scattering parameter r determines the trend of a theoretical model for Seebeck coefficient vs. carrier concentration. Equation 2.3.1

$$S = -\frac{k_B}{q}\left(\eta - \frac{(r+\frac{5}{2})F_{r+\frac{5}{2}}}{(r+\frac{3}{2})F_{r+\frac{5}{2}}}\right)$$

and 2.3.2

$$n = \frac{N_V}{2\pi^2}\left(\frac{2k_BTm_d}{\hbar^2}\right)^{3/2}F_{1/2}(\zeta^*)$$

are calculated using the Fermi-integral table located in Appendix A and the values of $r = 0$ and $r = -1/2$ for the scattering parameter to produce the dotted lines of theoretical values. N_V is the number of degenerate valleys, m_d is the density of states effective mass, and ζ^* is the reduced Fermi energy. All these values can be found in Appendix B. Once calculated, a table can be made of values correlating the measured data plotted against the theoretical values of carrier concentration and Seebeck coefficient. $r = 0$ and $r = -1/2$ are used to represent acoustic phonon scattering and neutral impurity scattering.

Figure 4.4 is plotted assuming a parabolic density of states and power-law dependence for the relaxation time, τ found in chapter 2.

Figure 4.4 shows the theoretical values of Seebeck coefficient vs. carrier concentration. It can be seen that the sample data does not follow the trend of the transport theory for standard bulk crystalline materials. They clearly must follow a different scattering parameter. This is evidence for low-energy electron filtering in the nano-composites.

Chapter 5

CONCLUSIONS

5.1 Conclusion

The experiments and techniques shown in this paper are the basics of electronic transport and are widely used in research. The Hall effect and Seebeck effect are excellent tools for characterizing semiconductor materials. These ideas carry over to the thermoelectric industry for ways of creating more efficient thermoelectric materials to be used in different applications.

The Hall effect is one of the mostly widely used experimental technique for semiconductors because of its ability to accurately determine carrier information. The effect outlined in this paper is evidence for that. When measuring the carrier concentration and mobility we are able to confirms the theory of enhancing the ZT of a thermoelectric.

The ZEM3 was utilized to measure the Seebeck coefficient of the Bi_2Te_3 samples, cut into rectangular prism, from room temperature (300K) to 423K. These samples were then measured in a Hall effect apparatus built from Lakeshore and GMW equipment. All samples measured in the Hall apparatus were done at room temperature and provided values of the Hall coefficient, carrier concentration, resistivity, and mobility.

Results show that increasing the carrier concentration without drastically changing the Seebeck coefficient will produce thermoelectric materials with a higher ZT. Nano-structured

Bi_2Te_3 with semi-metal bismuth nano-inclusions described here have shown evidence of a low-energy electron filtering effect. This effect is able to increase the ZT by increasing the carrier concentration but not changing the Seebeck effect.

Appendix A

FERMI INTEGRAL VALUES

η	$F_{-1/2}$	F_0	$F_{1/2}$	F_1	$F_{3/2}$
-2	0.21919	0.12693	0.11459	0.13101	0.17580
-1.8	0.26278	0.15298	0.13863	0.15893	0.21367
-1.6	0.31393	0.18390	0.16740	0.19253	0.25945
-1.4	0.37352	0.22042	0.20170	0.23286	0.31467
-1.2	0.44235	0.26328	0.24241	0.28112	0.38111
-1	0.52114	0.31326	0.29050	0.33865	0.46085
-0.8	0.61038	0.37110	0.34699	0.40695	0.55625
-0.6	0.71033	0.43749	0.41294	0.48766	0.66999
-0.4	0.82094	0.51302	0.48941	0.58255	0.80506
-0.2	0.94179	0.59814	0.57747	0.69350	0.96479
0	1.07213	0.69315	0.67809	0.82247	1.15280
0.2	1.21086	0.79814	0.79218	0.97143	1.37300
0.4	1.35662	0.91302	0.92051	1.14238	1.62954
0.6	1.50787	1.03749	1.06369	1.33727	1.92679
0.8	1.66299	1.17110	1.22221	1.55798	2.26928
1	1.82037	1.31326	1.39637	1.80628	2.66167
1.2	1.97851	1.46328	1.58632	2.08380	3.10867
1.4	2.13609	1.62041	1.79206	2.39205	3.61502
1.6	2.29197	1.78390	2.01348	2.73236	4.18544
1.8	2.44526	1.95297	2.25036	3.10594	4.82462
2	2.59528	2.12692	2.50241	3.51383	5.53714
2.2	2.74154	2.30507	2.76928	3.95693	6.32752
2.4	2.88374	2.48681	3.05058	4.43604	7.20015
2.6	3.02170	2.67161	3.35890	4.95181	8.15931
2.8	3.15539	2.85900	3.65479	5.50483	9.20915
3	3.28485	3.04855	3.97687	6.09556	10.35370

Table A.1: Fermi-Integral Values

η	F_2	$F_{5/2}$	F_3	$F_{7/2}$	F_4
-2	0.26627	0.44455	0.8053	1.5650	3.2345
-1.8	0.32408	0.54162	0.9819	1.9090	3.9471
-1.6	0.39416	0.65954	1.1967	2.3281	4.8157
-1.4	0.47900	0.80264	1.4578	2.8383	5.8741
-1.2	0.58151	0.97608	1.7750	3.4589	7.1631
-1	0.70513	1.18597	2.1598	4.2133	8.7321
-0.8	0.85386	1.43954	2.6262	5.1294	10.6406
-0.6	1.03234	1.74527	3.1904	6.2408	12.9601
-0.4	1.24588	2.11308	3.8720	7.5873	15.7765
-0.2	1.50052	2.55444	4.6937	9.2162	19.1926
0	1.80309	3.08259	5.6822	11.1837	23.3309
0.2	2.16116	3.71261	6.8685	13.5556	28.3369
0.4	2.58316	4.46164	8.2884	16.4092	34.3830
0.6	3.07826	5.34894	9.9830	19.8344	41.6723
0.8	3.65642	6.39600	11.9991	23.9356	50.4432
1	4.32833	7.62661	14.3898	28.8329	60.9745
1.2	5.10535	9.06691	17.2148	34.6643	73.5903
1.4	5.99949	10.74543	20.5409	41.5868	88.6657
1.6	7.02331	12.69308	24.4423	49.7786	106.6324
1.8	8.18990	14.94311	29.0009	59.4401	127.9849
2	9.51280	17.53113	34.3067	70.7962	153.2857
2.2	11.00594	20.49501	40.4578	84.0970	183.1721
2.4	12.68359	23.87484	47.5608	99.6198	218.3621
2.6	14.56031	27.71286	55.7307	117.6701	259.6599
2.8	16.65089	32.05334	65.0912	138.5827	307.9621
3	18.97031	36.94250	75.7744	162.7227	364.2625

Appendix B

BI2TE3 SOLID STATE CONSTANT VALUES

TABLE B.1: General properties of Bi_2Te_3

Property	Symbol	Value	Temperature
Hexagonal Unit	a	$(4.3835 \pm 0.0005) \times 10^{-10}m$	$20°C$
cell dimensions	c	$(30.487 \pm 0.001) \times 10^{-10}m$	$20°C$
Density	ρ_d	$(7.8587 \pm 0.0002) \times 10^3 kgm^{-3}$	$27°C$
Elastic constants	c_{11}	$6.46{\times}10^{10} Nm^{-2}$	$27°C$
	c_{12}	$3.58{\times}10^{10} Nm^{-2}$	$27°C$
	c_{33}	$4.73{\times}10^{10} Nm^{-2}$	$27°C$
	c_{44}	$2.5{\times}10^{10} Nm^{-2}$	
	c_{13}	not determined	
	c_{14}	not determined	
Specific heat (high T)		$1.507{\times}10^4 + 54.4T - 0.130T^2 JK^{-1}kg\text{–}mole^{-1}$	up to $550°C$
Specific heat (low T)		$0.84{\pm}0.37T + 2.33 \times 10^6 (T/\theta_D)^3 JK^{-1}kg\text{–}mole^{-1}$	below 2.3K
Latent heat of fusion		$(1.21 + 0.04) \times 10^8 Jkg\text{–}mole^{-1}$	
Debye Temp.	θ_D	$155.5 + 3K$	0K

TABLE B.2: Electrical, optical, and thermal properties of Bi_2Te_3

Property	Symbol	Value	T
Carrier mobility			
electrons	μ_n	$0.120 m^2 V^{-1} s^{-1}$	293K
holes	μ_p	$0.051 m^2 V^{-1} s^{-1}$	293K
Temperature dependence of mobility			
electrons		$\mu_n \alpha T^{-1.68}$	
holes		$\mu_p \alpha T^{-1.95}$	
Density-of-states effective mass:			
electrons	${m_n}^*$	0.37m	77K
	${m_n}^*$	0.58m	293K
holes	${m_p}^*$	0.51m	77K
	${m_p}^*$	1.07m	293K
Exponent in scattering law	r	-0.5	
Refractive index		9.2	
Lattice thermal conductiviy:	λ_L		
perpindicular to c-axis		$1.5 W m^{-1} K^{-1}$	300K
parallel to c-axis		$0.7 W m^{-1} K^{-1}$	300K

Appendix C

SEEBECK COEFFICIENT AND CARRIER CONCENTRATION VALUES

This appendix is for the values of the Seebeck coefficient and carrier concentration from chapter two theory. The Seebeck coefficient used to calculate the values is

$$S = -\frac{k_B}{q}\left(\eta - \frac{(r+\frac{5}{2})F_{r+\frac{5}{2}}}{(r+\frac{3}{2})F_{r+\frac{5}{2}}}\right) \tag{C.0.1}$$

and the carrier concentration

$$n = \frac{N^{2/3}{}_V m_d}{2\pi^2}\left(\frac{2k_B T m_d}{\hbar^2}\right)^{3/2} F_{1/2}(\zeta*) \tag{C.0.2}$$

The values were obtained by using step values of the reduced energy $\zeta = \frac{E}{k_B T}$. These values were ranging from 0.1 to 10 with step values of 0.1. Each column below, except carrier concentration, are separated by the scattering parameter, r, values ranging from 0 to 1 in half steps.

TABLE C.1: Seebeck coefficient and carrier concentration values for pisarenko plot.

n	S_0	$S_{1/2}$	S_1	$\|S_0\|$	$\|S_{1/2}\|$	$\|S_1\|$
0.91652	-237.743	-198.345	-157.541	237.7434	198.345	157.541
0.98998	-231.577	-192.438	-151.82	231.5772	192.4383	151.8195
1.06788	-225.553	-186.685	-146.262	225.5529	186.6847	146.2623
1.15034	-219.673	-181.086	-140.872	219.6731	181.0863	140.8716
1.23745	-213.94	-175.645	-135.649	213.9397	175.6446	135.6492
1.32928	-208.354	-170.361	-130.596	208.3539	170.3606	130.5959
1.42591	-202.917	-165.235	-125.712	202.9168	165.2347	125.7123
1.52738	-197.629	-160.267	-120.998	197.6288	160.2669	120.998
1.63375	-192.49	-155.457	-116.452	192.4898	155.4566	116.4525
1.74503	-187.499	-150.803	-112.074	187.4994	150.8026	112.0742
1.86125	-182.657	-146.303	-107.861	182.6565	146.3033	107.8613
1.9824	-177.96	-141.957	-103.812	177.9598	141.9568	103.8116
2.1085	-173.408	-137.761	-99.9221	173.4076	137.7606	99.92212
2.23952	-168.998	-133.712	-96.1898	168.9978	133.7121	96.18977
2.37544	-164.728	-129.808	-92.611	164.7281	129.8081	92.611
2.51624	-160.596	-126.045	-89.182	160.5957	126.0454	89.18197
2.66186	-156.598	-122.421	-85.8986	156.5978	122.4205	85.89861
2.81228	-152.731	-118.93	-82.7566	152.7313	118.9297	82.75662
2.96744	-148.993	-115.569	-79.7516	148.993	115.5691	79.75157
3.12728	-145.379	-112.335	-76.8789	145.3795	112.3347	76.87888
3.29176	-141.887	-109.223	-74.1339	141.8873	109.2227	74.13392
3.46081	-138.513	-106.229	-71.512	138.513	106.2288	71.51199
3.63436	-135.253	-103.349	-69.0084	135.253	103.3491	69.00838
3.81236	-132.104	-100.579	-66.6184	132.1035	100.5794	66.61842
3.99474	-129.061	-97.9158	-64.3375	129.0612	97.91582	64.33745
4.18143	-126.122	-95.3543	-62.1609	126.1223	95.35425	62.16089
4.37237	-123.283	-92.8908	-60.0842	123.2833	92.89082	60.08424
4.56748	-120.541	-90.5217	-58.1031	120.5408	90.52166	58.10309
4.76671	-117.891	-88.243	-56.2131	117.8912	88.24303	56.21314
4.96998	-115.331	-86.0513	-54.4102	115.3313	86.05125	54.41021
5.17723	-112.858	-83.9428	-52.6903	112.8577	83.94277	52.69026
5.3884	-110.467	-81.9141	-51.0494	110.4672	81.91414	51.04936
5.60343	-108.157	-79.962	-49.4837	108.1568	79.96201	49.48374
5.82225	-105.923	-78.0832	-47.9898	105.9232	78.08315	47.98977
6.04481	-103.764	-76.2745	-46.5639	103.7638	76.27445	46.56393
6.27104	-101.675	-74.5329	-45.2029	101.6754	74.53292	45.20289
6.50089	-99.6556	-72.8557	-43.9034	99.65557	72.85568	43.90342
6.7343	-97.7015	-71.24	-42.6625	97.70148	71.23995	42.66246
6.97121	-95.8106	-69.6831	-41.4771	95.81061	69.68308	41.47708

Table C.2: Seebeck coefficient and carrier concentration values for pisarenko plot.

n	S_0	$S_{1/2}$	S_1	$\|S_0\|$	$\|S_{1/2}\|$	$\|S_1\|$
7.21159	-93.9805	-68.1825	-40.3445	93.98052	68.18252	40.34447
7.45537	-92.2088	-66.7358	-39.262	92.20882	66.73584	39.26197
7.70251	-90.4933	-65.3407	-38.227	90.49325	65.34071	38.22703
7.95295	-88.8316	-63.9949	-37.2373	88.83161	63.99488	37.23725
8.20666	-87.2218	-62.6962	-36.2903	87.2218	62.69624	36.29032
8.46358	-85.6618	-61.4427	-35.3841	85.66182	61.44273	35.38406
8.72368	-84.1497	-60.2324	-34.5164	84.14972	60.23242	34.5164
8.98691	-82.6837	-59.0635	-33.6854	82.68365	59.06345	33.68538
9.25324	-81.2619	-57.934	-32.8891	81.26185	57.93404	32.88912
9.52261	-79.8826	-56.8425	-32.1259	79.88259	56.8425	32.12587
9.795	-78.5443	-55.7872	-31.394	78.54425	55.78722	31.39396
10.07037	-77.2453	-54.7667	-30.6918	77.24528	54.76666	30.69178
10.34868	-75.9842	-53.7794	-30.0179	75.98416	53.77936	30.01785
10.62989	-74.7595	-52.8239	-29.3708	74.75948	52.82391	29.37075
10.91399	-73.5699	-51.899	-28.7491	73.56985	51.89898	28.74912
11.20092	-72.414	-51.0033	-28.1517	72.41396	51.0033	28.1517
11.49066	-71.2906	-50.1357	-27.5773	71.29056	50.13566	27.57728
11.78319	-70.1984	-49.2949	-27.0247	70.19844	49.29491	27.02473
12.07847	-69.1364	-48.4799	-26.493	69.13644	48.47994	26.49296
12.37646	-68.1035	-47.6897	-25.981	68.10346	47.6897	25.98096
12.67716	-67.0985	-46.9232	-25.4878	67.09845	46.9232	25.48776
12.98052	-66.1204	-46.1795	-25.0125	66.12038	46.17948	25.01245
13.28653	-65.1683	-45.4576	-24.5542	65.1683	45.45763	24.55417
13.59515	-64.2413	-44.7568	-24.1121	64.24127	44.75678	24.11211
13.90636	-63.3384	-44.0761	-23.6855	63.3384	44.0761	23.68549
14.22015	-62.4588	-43.4148	-23.2736	62.45884	43.41482	23.27359
14.53648	-61.6018	-42.7722	-22.8757	61.60176	42.77217	22.87572
14.85533	-60.7664	-42.1474	-22.4912	60.7664	42.14743	22.49121
15.17668	-59.952	-41.5399	-22.1195	59.95199	41.53992	22.11946
15.50051	-59.1578	-40.949	-21.7599	59.15782	40.94899	21.75988
15.82681	-58.3832	-40.374	-21.4119	58.3832	40.37402	21.41192
16.15554	-57.6275	-39.8144	-21.075	57.62746	39.81439	21.07504
16.48669	-56.89	-39.2696	-20.7488	56.88998	39.26955	20.74877
16.82024	-56.1701	-38.739	-20.4326	56.17013	38.73896	20.43262
17.15617	-55.4674	-38.2221	-20.1262	55.46735	38.22208	20.12616
17.49446	-54.7811	-37.7184	-19.829	54.78106	37.71843	19.82895
17.8351	-54.1107	-37.2275	-19.5406	54.11072	37.22752	19.54061
18.17806	-53.4558	-36.7489	-19.2608	53.45583	36.74891	19.26075
18.52334	-52.8159	-36.2822	-18.989	52.81589	36.28216	18.98901
18.87091	-52.1904	-35.8269	-18.7251	52.19041	35.82685	18.72506

Table C.3: Seebeck coefficient and carrier concentration values for pisarenko plot.

n	S_0	$S_{1/2}$	S_1	$\|S_0\|$	$\|S_{1/2}\|$	$\|S_1\|$
19.22076	-51.5789	-35.3826	-18.4686	51.57894	35.38259	18.46856
19.57287	-50.981	-34.949	-18.2192	50.98103	34.949	18.21921
19.92723	-50.3963	-34.5257	-17.9767	50.39628	34.5257	17.97673
20.28382	-49.8243	-34.1124	-17.7408	49.82426	34.11236	17.74083
20.64262	-49.2646	-33.7086	-17.5113	49.26459	33.70863	17.51125
21.00362	-48.7169	-33.3142	-17.2878	48.71689	33.3142	17.28775
21.36682	-48.1808	-32.9288	-17.0701	48.1808	32.92876	17.07007
21.73218	-47.656	-32.552	-16.858	47.65596	32.55202	16.85801
22.09971	-47.1421	-32.1837	-16.6513	47.14205	32.18369	16.65134
22.46938	-46.6388	-31.8235	-16.4499	46.63875	31.8235	16.44986
22.84119	-46.1457	-31.4712	-16.2534	46.14573	31.47119	16.25338
23.21512	-45.6627	-31.1265	-16.0617	45.6627	31.12651	16.0617
23.59115	-45.1894	-30.7892	-15.8747	45.18937	30.78923	15.87466
23.96928	-44.7255	-30.4591	-15.6921	44.72547	30.45911	15.69209
24.34949	-44.2707	-30.1359	-15.5138	44.27072	30.13593	15.51381
24.73178	-43.8249	-29.8195	-15.3397	43.82486	29.81949	15.33969
25.11612	-43.3877	-29.5096	-15.1696	43.38766	29.50957	15.16958
25.50251	-42.9589	-29.206	-15.0033	42.95886	29.20598	15.00334
25.89094	-42.5382	-28.9085	-14.8408	42.53823	28.90852	14.84082
26.28139	-42.1256	-28.617	-14.6819	42.12555	28.61703	14.68192
26.67386	-41.7206	-28.3313	-14.5265	41.72061	28.33133	14.5265

Appendix D

LAKESHORE 370/3708 VOLTAGE RANGES

200 kΩ — resistance range
100 Ω — resolution
1.0 fw — power

TABLE D.1: Lakeshore 370/3708 Voltage Range

	6.32 mV	2.0 mV	632 μV	200 μV	63.2 μV	20 μV	6.32 μV	2.0 μV
31.6 mA	200 mΩ 200 nΩ 100 μW	63.2mΩ 63 nΩ 32 μW	20 mΩ 40 nΩ 10 μW	6.32 mΩ 13 nΩ 3.2 μW	2.0 mΩ 10 nΩ 1.0 μW	632 μΩ 10 nΩ 320 nW	200 μΩ 10 nΩ 100 nW	63.2 μΩ 10 nΩ 32 nW
10 mA	632 mΩ 630 nΩ 32 μW	200 mΩ 200 nΩ 10 μW	63.2 mΩ 130 nΩ 3.2 μW	20 mΩ 40 nΩ 1.0 μW	6.32 mΩ 32 nΩ 320 nW	2.0 mΩ 32 nΩ 100 nW	632 μΩ 32 nΩ 32 nW	200 μΩ 32 nΩ 10 nW
3.16 mA	2.0 Ω 2.0 μΩ 10 μW	632 mΩ 630 nΩ 3.2 μW	200 mΩ 400 nΩ 320 nW	63.2 mΩ 130 nΩ 320 nW	20 mΩ 100 nΩ 100 nW	6.32 mΩ 100 nΩ 32 nW	2.0 mΩ 100 nΩ 10 nW	632 μΩ 100 nΩ 3.2 nW
1.0 mA	6.32 Ω 6.3 μΩ 3.2 μW	2.0 Ω 2.0 μΩ 1.0 μW	632 mΩ 1.3 μΩ 320 nW	200 mΩ 400 nΩ 100 nW	63.2 mΩ 320 nΩ 32 nW	20 mΩ 320 nΩ 10 nW	6.32 mΩ 320 nΩ 3.2 nW	2.0 mΩ 320 nΩ 1.0 nW
316 μA	20 Ω 20 μΩ 1.0 μW	6.32 Ω 6.3 μΩ 320 nW	2 Ω 4.0 μΩ 100 nW	632 mΩ 1.3 μΩ 32 nW	200 mΩ 1.0 μΩ 10 nW	63.2 mΩ 1.0 μΩ 3.2 nW	20 mΩ 1.0 μΩ 1.0 nW	6.32 mΩ 1.0 μΩ 320 pW
100 μA	63.2 Ω 63 μΩ 320 nW	20 Ω 20 μΩ 100 nW	6.32 Ω 13 μΩ 32 nW	2 Ω 4.0 μΩ 10 nW	632 mΩ 3.2 μΩ 3.2 nW	200 mΩ 3.2 μΩ 1.0 nW	63.2 mΩ 3.2 mΩ 320 pW	20 mΩ 3.2 μΩ 100 pW

Table D.2: Lakeshore 370/3708 Voltage Range cont.

31.6 μA	200 Ω 200 μΩ 100 nW	63.2 Ω 63 μΩ 32 nW	20 Ω 40 μΩ 10 nW	6.32 Ω 13 μΩ 3.2 nW	2.0 Ω 10 μΩ 1.0 nW	632 mΩ 10 μΩ 320 pW	200 mΩ 10 μΩ 100 pW	63.2 mΩ 10 μΩ 32 pW
10 μA	632 Ω 630 μΩ 32 nW	200 Ω 200 μΩ 10 nW	63.2 Ω 130 μΩ 3.2 nW	20 Ω 40 μΩ 1.0 nW	6.32 Ω 32 μΩ 320 pW	2.0 Ω 32 μΩ 100 pW	632 mΩ 32 μΩ 32 pW	200 mΩ 32 μΩ 10 pW
3.16 μA	2.0 kΩ 2.0 m 10 nW	632 Ω 630 m 3.2 nW	200 Ω 400 μΩ 1.0 nW	63.2 Ω 130 μΩ 320 pW	20 Ω 100 μΩ 100 pW	6.32 Ω 100 μΩ 32 pW	2.0 Ω 100 μΩ 10 pW	632 mΩ 100 μΩ 3.2 pW
1.0 μA	6.32 kΩ 6.3 m 3.2 nW	2.0 kΩ 2.0 m 1.0 nW	632 Ω 1.3 m 320 pW	200 Ω 400 μΩ 100 pW	63.2 Ω 320 μΩ 32 pW	20 Ω 320 μΩ 10 pW	6.32 Ω 320 μΩ 3.2 pW	2.0 Ω 320 μΩ 1.0 pW
316 nA	20 kΩ 20 m 10 nW	6.32 kΩ 6.3 m 320 pW	2.0 kΩ 4.0 m 100 pW	632 Ω 1.3 m 32 pW	200 Ω 1.0 m 10 pW	63.2 Ω 1.0 m 3.2 pW	20 Ω 1.0 m 1.0 pW	6.32 Ω 1.0 m 320 fW
100 nA	63.2 kΩ 63 mΩ 320 pW	20 kΩ 40 mΩ 100 pW	6.32 kΩ 13 mΩ 32 pW	2.0 kΩ 6.0 mΩ 10 pW	632 Ω 3.2 mΩ 3.2 pW	200 Ω 3.2 mΩ 1.0 pW	63.2 Ω 3.2 mΩ 320 fW	20 Ω 3.2 mΩ 100 fW
31.6 nA	200 kΩ 400 mΩ 100 pW	63.2 kΩ 130 mΩ 32 pW	20 kΩ 60 mΩ 10 pW	6.32 kΩ 20 mΩ 3.2 pW	2.0 kΩ 20 mΩ 1.0 pW	632 Ω 10 mΩ 320 fW	200 Ω 10 mΩ 100 fW	63.2 Ω 10 mΩ 32 fW
10 nA	632 kΩ 1.9 Ω 32 pW	200 kΩ 600 mΩ 10 pW	63.2 kΩ 200 mΩ 3.2 pW	20 kΩ 200 mΩ 1.0 pW	6.32 kΩ 63 mΩ 320 fW	2.0 kΩ 63 mΩ 100 fW	632 Ω 32 mΩ 32 fW	200 Ω 32 mΩ 10 fW

Table D.3: Lakeshore 370/3708 Voltage Range cont.

3.16 nA	2.0 MΩ 6.0 Ω 10 pW	632 kΩ 2.0 Ω 3.2 pW	200 kΩ 2.0 Ω 1.0 pW	63.2 kΩ 630 mΩ 320 fW	20 kΩ 600 mΩ 100 fW	6.32 kΩ 200 mΩ 32 fW	2.0kΩ 200 mΩ 10 fW	632 Ω 100 mΩ 3.2 fW
1.0 nA	6.32 MΩ ** 3.2 pW	2.0 MΩ 20 Ω 1.0 pW	632 kΩ 6.3 Ω 320 fW*	200 kΩ 6.0 Ω 100 fW	63.2 kΩ 3.2Ω 32 fW	20 kΩ 2.0 Ω 10 fW	6.32 kΩ 630 mΩ 3.2 fW	2.0 kΩ 1.0 Ω 1.0 fW
316 pA	* * *	6.32 MΩ ** 320 fW	2.0 MΩ 60 Ω 100 fW	632 kΩ 19 Ω 32 fW	200 kΩ 20 Ω 10 fW	63.2 kΩ 6.3 Ω 3.2 fW	20 kΩ 3.0 Ω 1.0 fW	6.32 kΩ 3.2 Ω 320 aW
100 pA	* * *	* * *	6.32 MΩ ** 32 fW	2.0 MΩ 200 Ω 10 fW	632 kΩ 63 Ω 3.2 fW	200 kΩ 60 Ω 1.0 fW	63.2 kΩ 32 Ω 320 aW	20 kΩ 20 Ω 100 aW
31.6 pA	* * *	* * *	* * *	6.32 MΩ ** 3.2 fW	2.0 MΩ 600 Ω 1.0 fW	632 kΩ 190 Ω 320 aW	200 kΩ 200 Ω 100 aW	63.2 kΩ 63 Ω 32 aW
10 pA	* * *	* * *	* * *	* * *	6.32 MΩ ** 320 aW	2.0 MΩ 2.0 kΩ 100 aW	632 kΩ 630 Ω 32 aW	200 kΩ 600 Ω 10 aW
3.16 pA	* * *	* * *	* * *	* * *	* * *	6.32 MΩ ** 32 aW	2.0 MΩ 6.0 kΩ 10 aW	632 kΩ 1.9 kΩ 3.2 aW

Appendix E

LAKESHORE 455 RMS OPERATION RANGE

TABLE E.1: The Lakeshore 455 DPS Gaussmeter operation ranges from the Lakeshore 455 manual for the High Sensitivity Probe (HSE).

Gauss	Tesla	Oersted	Amp/meter
Range and Resolution	Range and Resolution	Range and Resolution	Range and Resolution
35.000 kG	3.5000 T	35.000 kOe	2.8000 MA/m
3.5000 kG	350.000 mT	3.5000 kOe	280.000 kA/m
350.00 G	35.000 mT	350.00 Oe	28.000 kA/m
35.000 G	3.5000 mT	35.000 Oe	2.8000 kA/m
3.5000 G	350.000 μT	3.5000 Oe	280.00 A/m

Appendix F

FIELD VS. GAP FOR GMW ELECTROMAGNET

This is the calibration curves done at the GMW facilities when shipped. It is done with 4 different size poles of 25mm, 50mm, 75mm, and 100mm. The poles used are 100mm.

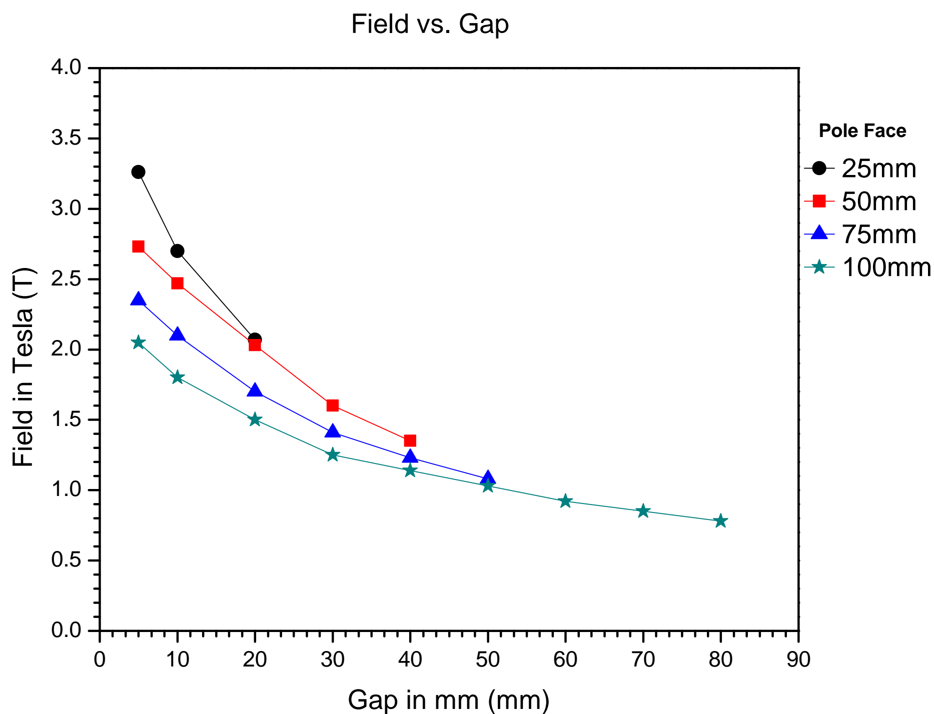

FIGURE F.1: This is the graph of pole distance vs. the magnetic field output.

Appendix G

CRM STAINLESS STEEL

This table is from the Certificate Standard Reference Materials 1460, 1461, and 1462. The stainless steel measured for this thesis is 1461 and was measured in bar form.[16] The value measured with the instruments described here is: $\rho = 773.85 n\Omega \cdot m$ at 300K. When compared to the values in the Certificate SRM, this value falls within 5% of the value below.

Table G.1: Table of thermal conductivity and electrical resistivity

T(K)	$\lambda(W \cdot m^{-1} \cdot K^{-1})$	$\rho(n\Omega \cdot m)$	T(K)	$\lambda(W \cdot m^{-1} \cdot K^{-1})$	$\rho(n\Omega \cdot m)$
2	0.152	593	40	5.01	595
3	0.249	593	45	5.57	597
4	0.352	593	50	6.08	599
5	0.462	594	60	6.98	606
6	0.575	594	70	7.72	613
7	0.693	594	80	8.34	622
8	0.814	594	90	8.85	630
9	0.938	594	100	9.3	639
10	1.064	594	150	10.94	683
12	1.323	594	200	12.2	724
14	1.588	594	250	13.31	767
16	1.858	593	300	14.32	810
18	2.132	593	400	16.16	885
20	2.407	593	500	17.78	944
25	3.092	592	600	19.23	997
30	3.763	592	700	20.54	1045
35	4.404	593	800	21.75	1088

Bibliography

[1] D.M. Rowe. *CRC Handbook of Thermoelectrics*. CRC Press, 1995. ISBN 9780849301469.

[2] E. H. Hall. On a new action of the magnet on electric currents. *American Journal of Mathematics*, 2(3):pp. 287–292, 1879. ISSN 00029327.

[3] The hall effect and related phenomena. *Solid-State Electronics*, 9(5):339 – 351.

[4] D.K. Schroder. *Semiconductor Material And Device Characterization*. IEEE Press, 2006. ISBN 9780471739067.

[5] G Jeffrey Snyder and Eric S Toberer. Complex thermoelectric materials. *Nature Materials*, 7(2):105–114, 2008.

[6] H J Goldsmid and R W Douglas. The use of semiconductors in thermoelectric refrigeration. *British Journal of Applied Physics*, 5(11):386, 1954.

[7] Enn Velmre. Thomas johann seebeck (1770-1831); 276-282. *Estonian Journal of Engineering*, 18(1):276–282, 2007. ISSN 1736-7522.

[8] S.B Riffat and Xiaoli Ma. Thermoelectrics: a review of present and potential applications. *Applied Thermal Engineering*, 23(8):913 – 935, 2003. ISSN 1359-4311. doi: 10.1016/S1359-4311(03)00012-7.

[9] Hadi Arabshahi. A new study on calculation of electron transport characteristics in semiconductor materials. *International Archive of Applied Sciences and Technology*, 1 (2):71–0, 2010.

[10] W.A. Harrison. *Solid State Theory*. Dover Books on Physics. Dover Publications, 1970. ISBN 9780486639482.

[11] J.D. Jackson. *Classical Electrodynamics*. Wiley, 1999. ISBN 9780471309321.

[12] S.S. Li. *Semiconductor physical electronics*. Microdevices : Physics and Fabrication Technologies. Springer, 2006. ISBN 9780387288932.

[13] S. Sumithra, Nathan J. Takas, Dinesh K. Misra, Westly M. Nolting, P. F. P. Poudeu, and Kevin L. Stokes. Enhancement in thermoelectric figure of merit in nanostructured bi2te3 with semimetal nanoinclusions. *Advanced Energy Materials*, 1(6):1141–1147, 2011.

[14] Lake Shore Cryogenics Inc. Appendix a - lake shore 7500/9500 hall system user manual.

[15] J. P. Fleurial, L. Gailliard, R. Triboulet, H. Scherrer, and S. Scherrer. Thermal properties of high quality single crystals of bismuth telluridepart i: Experimental characterization. *Journal of Physics and Chemistry of Solids*, 49, 1988.

[16] J.G. Hust abd A.B. Lankford. Austenitic stainless steel, thermal conductivity, and electrical resistivity as a function of temperature from 5 to 1200k, certificate standard reference materials 1460, 1461, 1462. *National Bureau of Standards*, 1984.

VITA

The author was born in New Orleans, Louisiana. He obtained his Bachelor of Science degree in Physics from the University of New Orleans in 2010. He joined the University of New Orleans physics graduate program to pursue a master's degree in applied physics, and became a member of the Stoke's research group in 2010.